Comput Geosci
DOI 10.1007/s10596-013-9371-1

ORIGINAL PAPER

Waterflooding optimization in uncertain geological scenarios

Andrea Capolei · Eka Suwartadi · Bjarne Foss · John Bagterp Jørgensen

Received: 21 March 2013 / Accepted: 21 August 2013

Abstract In conventional waterflooding of an oil field, feedback based optimal control technologies may enable higher oil recovery than with a conventional reactive strategy in which producers are closed based on water breakthrough. To compensate for the inherent geological uncertainties in an oil field, robust optimization has been suggested to improve and robustify optimal control strategies. In robust optimization of an oil reservoir, the water injection and production borehole pressures (bhp) are computed such that the predicted net present value (NPV) of an ensemble of permeability field realizations is maximized. In this paper, we both consider an open-loop optimization scenario, with no feedback, and a closed-loop optimization scenario. The closed-loop scenario is implemented in a moving horizon manner and feedback is obtained using an ensemble Kalman filter for estimation of the permeability field from the production data. For open-loop implementations, previous test case studies presented in the literature, show that a traditional robust optimization strategy (RO) gives a higher expected NPV with lower NPV standard deviation than a conventional reactive strategy. We present and study a test case where the opposite happen: The reactive strategy gives a higher expected NPV with a lower NPV standard deviation than the RO strategy. To improve the RO strategy, we propose a modified robust optimization strategy (modified RO) that can shut in uneconomical producer wells. This strategy inherits the features of both the reactive and the RO strategy. Simulations reveal that the modified RO strategy results in operations with larger returns and less risk than the reactive strategy, the RO strategy, and the certainty equivalent strategy. The returns are measured by the expected NPV and the risk is measured by the standard deviation of the NPV. In closed-loop optimization, we investigate and compare the performance of the RO strategy, the reactive strategy, and the certainty equivalent strategy. The certainty equivalent strategy is based on a single realization of the permeability field. It uses the mean of the ensemble as its permeability field. Simulations reveal that the RO strategy and the certainty equivalent strategy give a higher NPV compared to the reactive strategy. Surprisingly, the RO strategy and the certainty equivalent strategy give similar NPVs. Consequently, the certainty equivalent strategy is preferable in the closed-loop situation as it requires significantly less computational resources than the robust optimization strategy. The similarity of the certainty equivalent and the robust optimization based strategies for the closed-loop situation challenges the intuition of most reservoir engineers. Feedback reduces the uncertainty and this is the reason for the similar performance of the two strategies.

Keywords Robust optimization · Ensemble Kalman filter · Oil reservoir · Production optimization · Automatic history matching

A. Capolei · J. B. Jørgensen (✉)
Department of Applied Mathematics and Computer Science and Center for Energy Resources Engineering,
Technical University of Denmark (DTU),
2800 Kgs. Lyngby, Denmark
e-mail: jbjo@dtu.dk

A. Capolei
e-mail: acap@dtu.dk

E. Suwartadi · B. Foss
Department of Engineering Cybernetics,
Norwegian University of Science and Technology (NTNU),
7491 Trondheim, Norway

E. Suwartadi
e-mail: eka.suwartadi@ieee.org

B. Foss
e-mail: Bjarne.Foss@itk.ntnu.no

Published online: 17 September 2013

Mathematics Subject Classifications (2010) 90C30 · 49M37 · 49J20

1 Introduction

In the oil industry, closed-loop reservoir management (CLRM) has been suggested to maximize oil recovery or a financial measure such as the net present value of a given oil reservoir [1–12]. Fig. 1 illustrates the components in closed-loop reservoir management. The controller consists of model based data assimilation, also known as a parameter and state estimator, and a model based optimizer for maximizing the oil recovery or some predicted financial measure such as the net present value. The inputs to the controller is production measurements, forecasts of the oil price, the interest rate, and the operating unit costs. Based on these inputs the controller computes water injection trajectories as well as borehole pressure trajectories. Only the first part of these trajectories are implemented in the real oil reservoir. As new measurements become available, the process is repeated. The parameters and the states of the model are re-estimated using the data assimilation component. These filtered states and parameters are used in the model based optimization for computation of optimal trajectories for the manipulated variables, and the first part of the trajectories are implemented. This form of control is also known as Nonlinear Model Predictive Control (NMPC) [13–19]. A key difference of NMPC applied to reservoir management and traditional process control applications is the size of the model describing the system. In reservoir management, spatial discretization of the partial differential equation (PDE) system describing the flow results in a system of differential equations that is much larger than the systems typically encountered in process control applications. The large-scale nature of the closed-loop reservoir management problem requires special numerical techniques for the data assimilation [20] as well as the optimization [21, 22].

In this paper, we study and discuss two closed-loop approaches for real-time production optimization. Both of the two closed-loop approaches consist of three key elements: 1) A gradient based optimization algorithm for computation of the control input, 2) an ensemble Kalman filter (EnKF) for model updating through data assimilation (history-matching), and 3) use of the moving horizon principle for data assimilation and implementation of the computed control input.The first closed-loop approach is a certainty equivalent strategy. In this strategy, the EnKF is used to estimate permeabilities of each member of the ensemble. The average of these permeabilities is used in the optimization. The second closed-loop approach is a strategy based on robust optimization. In this strategy, all members of the ensemble are used to compute the mean net present value for the optimization.

We know from finance that strategies which attempt to increase returns are often accompanied by an increased uncertainty [23]. The robust strategy typically reduces the uncertainty of the expected outcome compared to a non-robust strategy and one would consequently expect a decrease in return [24, 25]. Figure 2 sketches this phenomenon. For the test cases used in the oil industry to test robust optimization strategies, this phenomenon has not been reported [26]. Due to the large-scale nature of an oil reservoir model, we cannot compute the entire distribution of the net present value for the closed-loop system. Accordingly, the ambition in this paper is in a computational tractable way, using a few realizations, to demonstrate the closed-loop performance of the certainty equivalent and the robust optimization strategy.

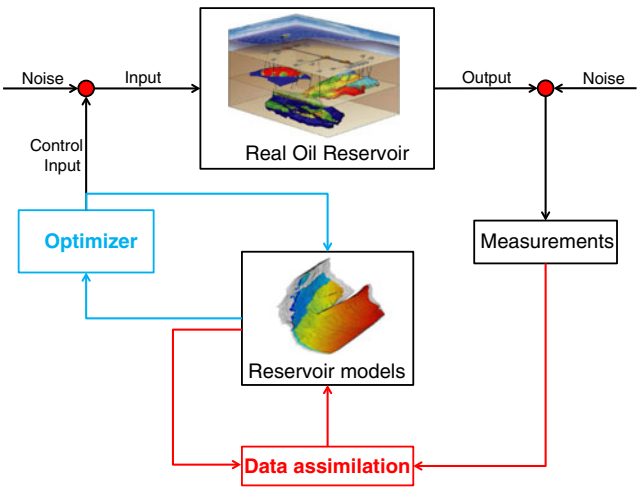

Fig. 1 Closed-loop reservoir management

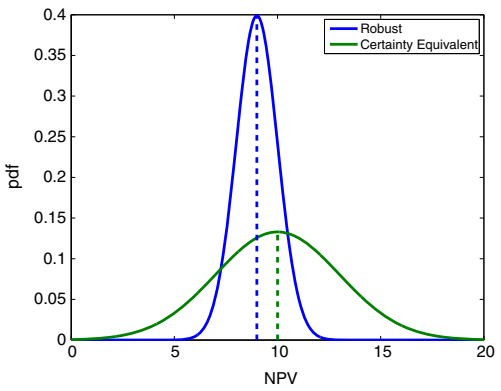

Fig. 2 Conceptual sketch of the distribution of the net present value for two strategies in finance. A robust strategy has lower variance and typically also lower mean value than non-robust strategies such as a certainty equivalent strategy

Data assimilation by the EnKF is a popular method for history matching as well as closed-loop reservoir management [1, 3, 4, 6, 27]. In [28], different data assimilation and optimization methods are tested on the synthetic "Brugge field" to maximize its NPV. The three best results are all obtained by methods using an EnKF for data assimilation. The EnKF method is a Monte Carlo implementation of the Kalman filter [29]. The literature available on the EnKF in petroleum engineering is rather large and mature. Data assimilation using the ensemble Kalman filter has been reviewed by [30–32] and [20, 33, 34] provide overviews of filtering techniques. A review of various issues of the EnKF, including sampling error because of small ensembles, covariance localization (limiting the influence of the observations to the state variables that are located spatially close to them), filter divergence, and model error, is given in [31] and [30]. [35] describes the necessity of introducing a confirming step to ensure consistency of the updated static and dynamic variables with the flow equations, while [30] discusses the reduction of the ensemble size with a resampling scheme. The problem of ensemble collapse is discussed in [36]. [37] considers a way to handle model constraints within the EnKF. [38] investigates an update step that preserves multi-point statistics and not only two point-statistics.

In the model based optimization part of CLRM, a traditional choice is to use methods based on one realization, usually the ensemble mean from the EnKF. To reduce the risk arising from uncertainty in the geological description, [26] proposes to optimize the expectation of net present value over a set of reservoir models using a gradient based method. This procedure is referred to as robust optimization (RO). In open-loop simulations, [26] compares the results of the RO procedure to two alternative approaches: a nominal optimization (NO) and a reactive control approach. They find that RO yields a much smaller variance than the alternatives. Moreover the RO strategy significantly improves the expected NPV over the alternative methods (on average 9.5 % higher than using reactive-control and 5.9 % higher than the average of NO strategies). [27, 39, 40] do closed-loop reservoir management using an EnKF for data assimilation and robust optimization with a gradient-free ensemble based optimization scheme for the model based optimization. [39] reports that an ensemble based optimization results in a NPV improvement of 22 % compared to a reactive strategy. However, they do not compare the closed-loop robust strategy to a closed-loop certainty equivalent strategy.

To our knowledge, there is no closed-loop application of the gradient-based robust optimization strategy as implemented in [26] available in the literature. Furthermore, the CLRM literature misses an open-loop as well as a closed-loop comparison of the performance of an ensemble based optimization scheme [39] or a gradient-based robust optimization scheme [26] with a certainty equivalent optimization strategy based on the ensemble mean. In this work we partially fill this gap and do CLRM comparing a RO strategy [26] to three alternative approaches: a reactive strategy, a nominal strategy, and a certainty equivalent strategy. By using feedback, the ensemble of permeability fields converge to a point such that the RO strategy becomes equivalent to the certainty equivalent strategy based on the ensemble mean. The RO is more expensive computationally than the certainty equivalent strategy. In this paper, we use a case study to compare the RO strategy in closed-loop to other strategies.

The paper is organized as follows. Section 2 defines the reservoir model. Section 3 states the constrained optimal control problem and describes the robust optimization strategy. The ensemble Kalman filter for data assimilation is described in Section 4. Section 5 describes the numerical case study and conclusions are presented in Section 6.

2 Reservoir model

In this work, we assume that the reservoirs are in the secondary recovery phase where the pressures are above the bubble point pressure of the oil phase. Therefore, two-phase immiscible flow, i.e. flow without mass transfer between the two phases, is a reasonable assumption. We focus on water-flooding cases for two-phase (oil and water) reservoirs. Further, we assume incompressible fluids and rocks, no gravity effects or capillary pressure, no-flow boundaries, constant porosity, and finally isothermal conditions. The state equations in an oil reservoir Ω, with boundary $\partial\Omega$ and outward facing normal vector $\mathbf{n}$, can be represented by pressure and saturation equations. The pressure equation is described as

$$\begin{aligned} \mathbf{v} &= -\lambda_t \mathbf{K}\nabla p, \qquad \nabla\cdot\mathbf{v} = q \qquad \text{in } \Omega \\ \mathbf{v}\cdot\mathbf{n} &= 0 \qquad \text{on } \partial\Omega \end{aligned} \tag{1}$$

$\mathbf{v}$ is the Darcy velocity (total velocity), $\mathbf{K}$ is the permeability, p is the pressure, q is the volumetric well rate, and λ_t is the total mobility, which in this setting is the sum of the water and oil mobility functions,

$$\lambda_t = \lambda_w(s) + \lambda_o(s) = k_{rw}(s)/\mu_w + k_{ro}(s)/\mu_o \tag{2}$$

The saturation equation is given by

$$\boldsymbol{\phi}\frac{\partial}{\partial t}S_w + \nabla\cdot\big(f_w(S_w)\mathbf{v}\big) = \frac{q_w}{\boldsymbol{\rho}_w} \tag{3}$$

$\boldsymbol{\phi}$ is the porosity, s is the saturation, $f_w(s)$ is the water fractional flow which is defined as $\frac{\lambda_w}{\lambda_t}$, and q_w is the volumetric water rate at the well. We use the MRST [41] reservoir simulator to solve the pressure and saturation equations,

(1) and (3), sequentially. Wells are implemented using the Peaceman well model [42]

$$q_i = -\lambda_t W I_i \left(p_i - p_i^{BHP} \right) \tag{4}$$

q_i is the flow rate into grid block i, p_i^{BHP} is the wellbore pressure, and WI_i is the Peaceman well-index.

3 Production optimization

Production optimization aims at maximizing a performance index, net present value or oil recovery, for the life time of the oil reservoir. Spatial and temporal discretization of the model equations and the performance index yield a finite dimensional nonlinear constrained optimization problem on a time horizon from 0 to N that can be formulated as

$$\max_{\{x_k\}_{k=0}^{N}, \{u_k\}_{k=0}^{N-1}} J = \sum_{k=0}^{N-1} J_k(x_k, x_{k+1}, u_k) \tag{5a}$$

subject to

$$x_0 = \bar{x}_0 \tag{5b}$$

$$g_k(x_k, x_{k+1}, u_k; \boldsymbol{\theta}) = 0 \qquad k \in \mathcal{N} := \{0, 1, \ldots, N-1\} \tag{5c}$$

$$c\left(\{u_k\}_{k=0}^{N-1} \right) \leq 0 \tag{5d}$$

$\bar{x}_0$ is the initial states, $\boldsymbol{\theta}$ is a parameter vector in an uncertain space $\boldsymbol{\Theta}$ (in our case the permeability field), x_k is the state vector, u_k is a piecewise constant control vector, g_k is the discretization of the dynamical model, (1) and (3), and $c\left(\{u_k\}_{k=0}^{N-1} \right)$ are linear bounds on the control vector. In our formulations we do not allow nonlinear state or output constraints, see e.g. [43].

3.1 Objective function

The optimizer maximizes the net present value by manipulating the well bhps. Hence, the manipulated variable at time period $k \in \mathcal{N}$ is $u_k = \left\{ \{p_{i,k}^{bhp}\}_{i \in \mathcal{I}}, \{p_{i,k}^{bhp}\}_{i \in \mathcal{P}} \right\}$ with $\mathcal{I}$ being the set of injectors and $\mathcal{P}$ being the set of producers. For $i \in \mathcal{I}$, $p_{i,k}^{bhp}$ is the bhp (bar) in time period $k \in \mathcal{N}$ at injector i. For $i \in \mathcal{P}$, $p_{i,k}^{bhp}$ is the bhp (bar) at producer i in time period $k \in \mathcal{N}$.

The stage cost, J_k, in the objective function for a net present value (NPV) maximization can be expressed as

$$J_k = -\frac{\Delta t_k}{(1+d)^{\frac{t_{k+1}}{\tau}}} \left[\sum_{i \in \mathcal{P}} r_o \, q_{o,i}^{k+1}(u_k, x_{k+1}) - \sum_{i \in \mathcal{P}} r_{wp} \, q_{w,i}^{k+1}(u_k, x_{k+1}) + \sum_{l \in \mathcal{I}} r_{wi} \, q_l^{k+1}(u_k, x_{k+1}) \right] \tag{6}$$

r_o, r_{wp}, and r_{wi} represent the oil price, the water separation cost, and the water injection cost, respectively. The water flow rate (bbl/day) in producer i at time period k is $q_{w,i}^k = f_w q_i^k$ and the oil flow rate is $q_{o,i}^k = (1 - f_w) q_i^k$. q_i^k is the flow rate at producer i as given by (4). The well rates at the injector wells are denoted by q_l (only water is injected). Note that from the well model (4), it follows that the flow rates q are negative for the producer wells and positive for the injector wells. d is the discount factor, Δt_k is the time interval, and N is the number of control steps. Note that in the special case when the discount factor is zero ($d = 0$) and the water injection and separation costs are zero as well, the NPV is equivalent to the quantity of produced oil.

3.2 Control and constraints

We control the bhp of the wells and assume that these control inputs are piecewise constant functions. The bhps are constrained by well and reservoir conditions. To maintain the two phase situation we require the pressure to be above the bubble point pressure (290 bar). To avoid fracturing the rock, the pressure must be below the fracture pressure of the rock (350 bar). To maintain flow from the injectors to the producers, the injection pressure is maintained above 310 bar and the producer pressures are kept below 310 bar. With these bounds we did not experience that the flow was reversed. Without these pressure bounds, however, state constraints, like bounds on flow rates (4), must be applied to avoid flow reversion.

3.3 Single-shooting optimization

We use a single shooting algorithm [11, 44] for solution of (5a). Alternatives are multiple-shooting [45, 46] and collocation methods [47]. Despite the fact that the multiple shooting and the collocation methods offer better convergence properties than the single-shooting method [45–47], their application in production optimization is restricted by the large state dimension of such problems. The use of multiple-shooting is prevented by the need for computation of state sensitivities. The collocation method do not allow for adaptive time stepping and would need to solve huge-scale optimization problems. In

the single shooting optimization algorithm, we define the function

$$\begin{aligned}\boldsymbol{\psi} &= \boldsymbol{\psi}\left(\{u_k\}_{k=0}^{N-1}; \bar{x}_0, \boldsymbol{\theta}\right) \\ &= \left\{ J = \sum_{k=0}^{N-1} J_k(x_k, x_{k+1}, u_k) : \right. \\ &\qquad \left. x_0 = \bar{x}_0, \quad g_k(x_k, x_{k+1}, u_k; \boldsymbol{\theta}) = 0,\ k \in \mathcal{N} \right\} \end{aligned} \tag{7}$$

such that (5a) can be expressed as the optimization problem

$$\begin{aligned} \max_{\{u_k\}_{k=0}^{N-1}} \quad & \boldsymbol{\psi} = \boldsymbol{\psi}\left(\{u_k\}_{k=0}^{N-1}; \bar{x}_0, \boldsymbol{\theta}\right) \\ s.t. \quad & c\left(\{u_k\}_{k=0}^{N-1}\right) \le 0 \end{aligned} \tag{8}$$

Gradient based optimization algorithms for solving (8) require evaluation of $\boldsymbol{\psi} = \boldsymbol{\psi}\left(\{u_k\}_{k=0}^{N-1}; \bar{x}_0, \boldsymbol{\theta}\right)$, $\nabla_{u_k}\boldsymbol{\psi}$ for $k \in \mathcal{N}$, $c\left(\{u_k\}_{k=0}^{N-1}\right)$, and $\nabla_{u_k} c\left(\{u_k\}_{k=0}^{N-1}\right)$ for $k \in \mathcal{N}$. The constraint function is in the cases considered linear bounds such that evaluation of these constraint functions and their gradients is trivial. Given an iterate, $\{u_k\}_{k=0}^{N-1}$, $\boldsymbol{\psi}$ is computed by solving (7) marching forwards. $\nabla_{u_k}\boldsymbol{\psi}$ for $k \in \mathcal{N}$ is computed by the adjoint method [9, 11, 43, 48–51]. In this method, the gradients $\{\nabla_{u_k}\boldsymbol{\psi}\}_{k=0}^{N-1}$ are computed using Algorithm 1 with

$$\nabla_{x_k} g_k = \nabla_{x_k} g_k(x_k, x_{k+1}, u_k; \boldsymbol{\theta}) \quad k \in \mathcal{N} \tag{9a}$$

$$\nabla_{x_{k+1}} g_k = \nabla_{x_{k+1}} g_k(x_k, x_{k+1}, u_k; \boldsymbol{\theta}) \quad k \in \mathcal{N} \tag{9b}$$

$$\nabla_{u_k} g_k = \nabla_{u_k} g_k(x_k, x_{k+1}, u_k; \boldsymbol{\theta}) \quad k \in \mathcal{N} \tag{9c}$$

$$\nabla_{x_k} J_k = \nabla_{x_k} J_k(x_k, x_{k+1}, u_k) \quad k \in \mathcal{N} \setminus \{0\} \tag{9d}$$

$$\nabla_{x_{k+1}} J_k = \nabla_{x_{k+1}} J_k(x_k, x_{k+1}, u_k) \quad k \in \mathcal{N} \tag{9e}$$

$$\nabla_{u_k} J_k = \nabla_{u_k} J_k(x_k, x_{k+1}, u_k) \quad k \in \mathcal{N} \tag{9f}$$

that are computed and stored during the forward solution of (7).

Algorithm 1 Adjoint method for computing $\{\nabla_{u_k}\boldsymbol{\psi}\}_{k=0}^{N-1}$.

Solve for λ_N in $\nabla_{x_N} g_{N-1}\lambda_N = \nabla_{x_N} J_{N-1}$
for $k = N-1, N-2, \ldots, 1$ **do**
  Compute $\nabla_{u_k}\boldsymbol{\psi} = \nabla_{u_k} J_k - \nabla_{u_k} g_k \lambda_{k+1}$
  Solve for λ_k in $\nabla_{x_k} g_{k-1}\lambda_k = \nabla_{x_k} J_{k-1} + \nabla_{x_k} J_k - \nabla_{x_k} g_k \lambda_{k+1}$
end for
Compute $\nabla_{u_0}\boldsymbol{\psi} = \nabla_{u_0} J_0 - \nabla_{u_0} g_0 \lambda_1$

To solve (8), we use two commercial optimization software packages: Knitro [52] and Matlab's `fmincon` function [53]. Knitro as well as `fmincon`, allows us to use an interior point or an active-set methods. We use up to 10 different initial guesses when running the optimizations and we find similar qualitative results with both software packages. Further, similar results are found with interior point and active-set methods. When using Knitro as well as `fmincon`, we select an interior point method since we experience the lowest computation times with this method. A local optimal solution is reported if the KKT conditions are satisfied to within a relative and absolute tolerance of 10^{-6}. The current best but non-optimal iterate is also returned in cases when the optimization algorithm uses more than 100 iterations. Similarly, the current best, but non-optimal, iterate is also returned in the case of a relative cost function or step size change less than 10^{-8}. Furthermore, in our simulations we noted that normalizing the cost function improved the convergence.

3.4 Certainty-equivalent and robust optimization

In certainty equivalent optimization, (8) is solved using the expected value for the parameters, $\boldsymbol{\eta} = E[\boldsymbol{\theta}]$, such that the objective used in (8) is

$$\boldsymbol{\psi}_{CE} = \boldsymbol{\psi}\left(\{u_k\}_{k=0}^{N-1}; \bar{x}_0, \boldsymbol{\eta}\right) \tag{10}$$

[26] introduces robust optimization to reduce the effect of geological uncertainties in the field development phase. Robust optimization uses a set of realizations that reflect the range of possible geological structures honoring the statistics of the geological uncertainties. In reservoir models, geological uncertainty is generally profound because of the noisy and sparse nature of seismic data, core samples, and borehole logs. The consequence of a large number of uncertain model parameters ($\boldsymbol{\theta}$) is the broad range of possible models that may satisfy the seismic and core-sample data. Nevertheless, in many cases, a single reservoir model is adopted in which the uncertain parameters, $\boldsymbol{\theta}$, are converted to deterministic parameters $\boldsymbol{\eta}$ by taking their expected values (i.e. $\boldsymbol{\eta} = E[\boldsymbol{\theta}]$). However, because the NPV is used as our measure of performance, we are more interested in the expected NPV over the uncertainty space, Θ (spanned by the uncertain parameters $\boldsymbol{\theta}$), than the mean of the parameters. The expected NPV over the uncertainty space, Θ, is in general not the same as the NPV computed using the expected values of the uncertain parameters, $\boldsymbol{\eta} = E[\boldsymbol{\theta}]$, as NPV is a nonlinear function of the parameters, $\boldsymbol{\theta}$. Consequently

$$\begin{aligned} E_{\boldsymbol{\theta}} & \left[\boldsymbol{\psi}\left(\{u_k\}_{k=0}^{N-1}; \bar{x}_0, \boldsymbol{\theta}\right)\right] \\ & \neq \boldsymbol{\psi}\left(\{u_k\}_{k=0}^{N-1}; \bar{x}_0, E_{\boldsymbol{\theta}}[\boldsymbol{\theta}]\right),\ \boldsymbol{\theta} \in \Theta \end{aligned} \tag{11}$$

Consider a discretization, $\Theta_d = \{\boldsymbol{\theta}_1, \ldots, \boldsymbol{\theta}_{n_d}\}$, of the uncertainty space, Θ, such that expected NPV may be approximated by

$$E_{\boldsymbol{\theta}} \left[\boldsymbol{\psi} \left(\{u_k\}_{k=0}^{N-1}; \bar{x}_0, \boldsymbol{\theta} \in \Theta \right) \right] \approx E_{\boldsymbol{\theta}} \left[\boldsymbol{\psi} \left(\{u_k\}_{k=0}^{N-1}; \bar{x}_0, \boldsymbol{\theta} \in \Theta_d \right) \right] \tag{12}$$

This approximation of the expected NPV is a better approximation than the NPV computed using the expected parameters, $\boldsymbol{\eta}$. In the special case of equiprobable realizations, the right-hand side of (12) is the arithmetic average

$$E_{\boldsymbol{\theta}} \left[\boldsymbol{\psi} \left(\{u_k\}_{k=0}^{N-1}; \bar{x}_0, \boldsymbol{\theta} \in \Theta_d \right) \right] = \frac{1}{n_d} \sum_{i=1}^{n_d} \boldsymbol{\psi} \left(\{u_k\}_{k=0}^{N-1}; \bar{x}_0, \boldsymbol{\theta}^i \right) \tag{13}$$

The robust optimization method uses the ensemble average as its objective function in (8)

$$\boldsymbol{\psi}_{rob} = \frac{1}{n_d} \sum_{i=1}^{n_d} \boldsymbol{\psi} \left(\{u_k\}_{k=0}^{N-1}; \bar{x}_0, \boldsymbol{\theta}^i \right) = \frac{1}{n_d} \sum_{i=1}^{n_d} \boldsymbol{\psi}^i \tag{14}$$

The corresponding gradients may be computed by

$$\nabla_{u_k} \boldsymbol{\psi}_{rob} = \frac{1}{n_d} \sum_{i=1}^{n_d} \nabla_{u_k} \boldsymbol{\psi} \left(\{u_k\}_{k=0}^{N-1}; \bar{x}_0, \boldsymbol{\theta}^i \right) \quad k \in \mathcal{N} \tag{15}$$

Compared to a certainty-equivalent computation, the computation of the robust cost function (14) and its gradient (15) results in an increased computational effort by a factor n_d. As the addends in these computations are decoupled, they can be computed in parallel.

3.5 Permeability field

In our study, the uncertainty lies in the permeability field. We generate 100 permeability field realizations of a 2D reservoir in a fluvial depositional environment with a known vertical main-flow direction, see Fig. 3. To generate the permeability fields we started by creating a set of 100 binary (black and white) training images by using the sequential Monte Carlo algorithm 'SNESIM' [54]. Then a Kernel PCA [55] procedure is used to preserves the channel structures and smooths the original binary images. The realizations so obtained are quite heterogeneous with permeabilities in the range $6 - 2734$ mD.

4 Ensemble Kalman filter

We use the Ensemble Kalman filter (EnKF) for estimating the permeability field based on production data measurements. The EnKF is a Monte Carlo implementation of the Kalman filter [13, 56–58] using an ensemble of n_d realizations to represent the necessary first and second moments (means and covariances). In this section we describe the EnKF.

Consider the discrete time system

$$\mathbf{x}_{k+1} = F(\mathbf{x}_{k,u_k,\boldsymbol{\theta}}) \tag{16a}$$

$$\mathbf{y}_k = G(\mathbf{x}_{k,u_k}) + \mathbf{v}_k \qquad \mathbf{v}_k \sim N(0, R) \tag{16b}$$

The dynamic equation (16a) is a representation of the model dynamics (5c) in explicit form. It should be noted that in this representation we do not consider stochastic model errors (process noise) [20]. The uncertain parameters $\boldsymbol{\theta}$ are the logarithm of the permeability field, $\boldsymbol{\theta} = \log(K)$. The states are the pressure and water saturation in each grid block, $x = [P; S_w]$. The initial states, x_0, can also be considered uncertain. However, in this work we fix them to their average value. u_k is the control input which represents the borehole pressures.

The measurements, y, are the fractional flow for each producer well and the water injection rate for each injector well. In the measurement equation (16b), $G(x_k, u_k)$ includes the Peaceman well model (4) as well as the equations relating fractional flow to pressures and water saturations. v_k is measurement noise that we assume is normally distributed.

4.1 Basic Ensemble Kalman filter

(16a) includes the states, x, and the parameters, $\boldsymbol{\theta}$. Therefore, we form the augmented state space model

$$\boldsymbol{x}_{k+1} = F(\boldsymbol{x}_k, u_k, \boldsymbol{\theta}_k) \tag{17a}$$

$$\boldsymbol{\theta}_{k+1} = \boldsymbol{\theta}_k \tag{17b}$$

and apply the EnKF to the dynamic equation (17a) and the measurement equation (16b). In the EnKF all means and covariances are represented by samples of the stochastic variables. Therefore, the initial mean and covariance of the augmented states, $[x_k, \boldsymbol{\theta}_k]$, are represented by

$$\{x^i_{0|0}, \boldsymbol{\theta}^i_{0|0}\}_{i=1}^{n_d} = \left\{ x_0, \boldsymbol{\theta}^i_{0|0} \right\}_{i=1}^{n_d} \tag{18}$$

It should be noted that the initial states, x_0, in our case are assumed to be known exactly. Only the parameters, $\boldsymbol{\theta}$, are uncertain. Index i refers to each of the n_d members of the ensemble, i.e. each realization.

In the following we describe the algorithm for discrete time instant $k = 1, 2, \ldots$. In general, at discrete time instant k, both the states and the parameters from the previous instant, $k-1$, are uncertain. This is denoted

$$\left\{ x^i_{k-1|k-1}, \boldsymbol{\theta}^i_{k-1|k-1} \right\}_{i=1}^{n_d} \quad k = 1, 2, \ldots \tag{19}$$

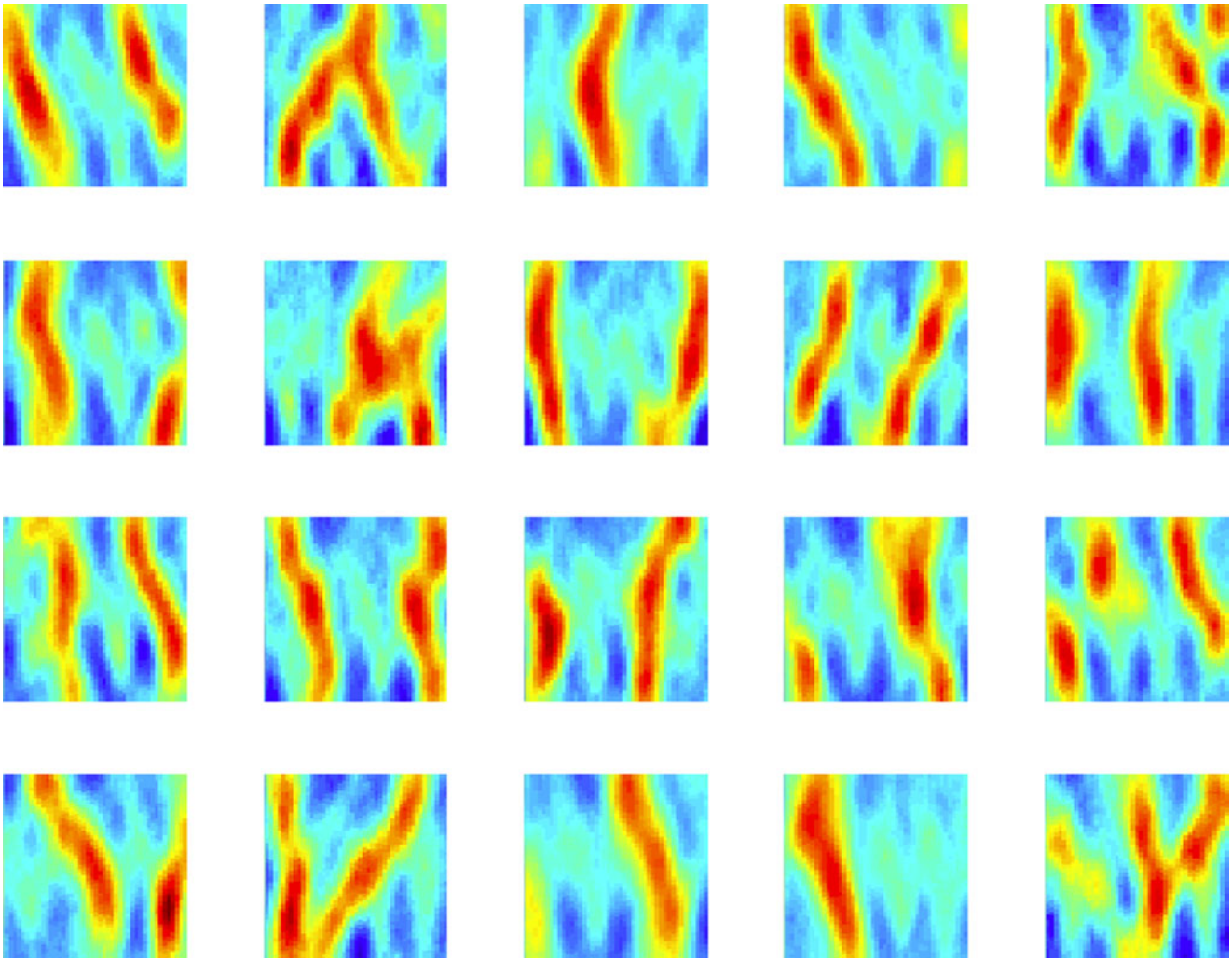

Fig. 3 A selection of realizations from the ensemble of 100 permeability fields. The realizations are quite heterogeneous, values are in the range $6 - 2734$ mD

In the EnKF, the one-step prediction step is conducted by passing each ensemble member through the dynamics (17a) such that for $i = 1, 2, \ldots, n_d$

$$x^i_{k|k-1} = F\left(x^i_{k-1|k-1}, u_{k-1}, \boldsymbol{\theta}^i_{k-1|k-1}\right), \tag{20a}$$

$$\boldsymbol{\theta}^i_{k|k-1} = \boldsymbol{\theta}^i_{k-1|k-1}, \tag{20b}$$

where the previous input, u_{k-1}, is known. Then the output, $z^i_{k|k-1}$, and the measurement, $y^i_{k|k-1}$, at discrete time k may be computed as

$$z^i_{k|k-1} = G\left(x^i_{k|k-1}, u_{k-1}\right) \qquad i = 1, 2, \ldots, n_d \tag{21a}$$

$$y^i_{k|k-1} = z^i_{k|k-1} + v^i_k \qquad i = 1, 2, \ldots, n_d \tag{21b}$$

To obtain the correct covariances of the state estimates in the EnKF, it is important that each ensemble member, $y^i_{k|k-1}$, contain measurement noise, $v^i_{k|k-1}$ [59]. It should also be noted that u_{k-1} is used in the evaluation of G in (21a). The explanation for the use of u_{k-1} is that we use a zero-order-hold representation of $u(t)$, i.e. $u(t) = u_{k-1}$ for $t_{k-1} \leq t < t_k$, and that we assume the measurement is conducted at time $t_k^- = \lim_{t<t_k} t$. Then, at time t_k, the EnKF and optimal control computations are conducted infinitely fast such the next decisions, $u(t) = u_k$ for $t_k \leq t < t_{k+1}$, can be implemented at time t_k.

The innovation, e^i_k, for each ensemble member is computed using the actual measurement, y_k, and the predicted measurement

$$\boldsymbol{\varepsilon}^i_k = z^i_{k|k-1} - y_k \qquad i = 1, 2, \ldots, n_d \tag{22a}$$

$$e^i_k = y_k - y^i_{k|k-1} = -\boldsymbol{\varepsilon}^i_k - v^i_k \qquad i = 1, 2, \ldots, n_d \tag{22b}$$

In these equations, y_k is the actual measurement and therefore a deterministic variable. In the EnKF, the realized trajectory of the system and an ensemble of different

Table 1 Parameters for the two phase model, the discounted state cost function (6), and the measurement noise

Symbol	Description	Value	Unit
ϕ	Porosity	0.2	–
c_r	Rock compressibility	0	Pa^{-1}
ρ_o	Oil density (300 bar)	700	kg/m^3
ρ_w	Water density (300 bar)	1000	kg/m^3
μ_o	Dynamic oil viscosity	$3 \cdot 10^{-3}$	$\text{Pa} \cdot \text{s}$
μ_w	Dynamic water viscosity	$0.3 \cdot 10^{-3}$	$\text{Pa} \cdot \text{s}$
S_{or}	Residual oil saturation	0.1	–
S_{ow}	Connate water saturation	0.1	–
n_o	Corey exponent for oil	2	–
n_w	Corey exponent for water	2	–
P_{init}	Initial reservoir pressure	300	bar
S_{init}	Initial water saturation	0.1	–
r_o	Oil price	120	USD/bbl
r_{wp}	Water production cost	20	USD/bbl
r_{wi}	Water injection cost	10	USD/bbl
d	Discount factor	0	–
R	Cov. matrix for measurements noises	Diag($5 \cdot 10^{-3}, 5 \cdot 10^{-3}, 5 \cdot 10^{-3}, 5 \cdot 10^{-3}, 30$)	

state trajectories are considered. In the derivation of the standard Kalman filter [13, 57, 58], it is the other way around. A (infinite) number of system realizations are considered, while the filter is represented by one deterministic trajectory (the mean).

The optimal linear estimator conditioned on the innovations are [57]

$$x^i_{k|k} = x^i_{k|k-1} + K_{x,k} e^i_k \qquad i = 1, 2, \ldots, n_d \tag{23a}$$

$$\boldsymbol{\theta}^i_{k|k} = \boldsymbol{\theta}^i_{k|k-1} + K_{\boldsymbol{\theta},k} e^i_k \qquad i = 1, 2, \ldots, n_d \tag{23b}$$

with the Kalman filter gains computed as

$$K_{x,k} = \langle x_{k|k-1}, e_k \rangle \langle e_k, e_k \rangle^{-1} \tag{24a}$$

$$K_{\boldsymbol{\theta},k} = \langle \boldsymbol{\theta}_{k|k-1}, e_k \rangle \langle e_k, e_k \rangle^{-1} \tag{24b}$$

using the covariances

$$\langle x_{k|k-1}, e_k \rangle = \langle x_{k|k-1}, \boldsymbol{\varepsilon}_k \rangle \tag{25a}$$

$$\langle \boldsymbol{\theta}_{k|k-1}, e_k \rangle = \langle \boldsymbol{\theta}_{k|k-1}, \boldsymbol{\varepsilon}_k \rangle \tag{25b}$$

$$\langle e_k, e_k \rangle = \langle \boldsymbol{\varepsilon}_k, \boldsymbol{\varepsilon}_k \rangle + \langle v_k, v_k \rangle \approx \langle \boldsymbol{\varepsilon}_k, \boldsymbol{\varepsilon}_k \rangle + R \tag{25c}$$

The Kalman gains may be based on direct computation of the empirical estimates ($\langle x_{k|k-1}, e_k \rangle$, $\langle \boldsymbol{\theta}_{k|k-1}, e_k \rangle$, $\langle e_k, e_k \rangle$) or the relations in (25a). We choose to base the computations on (25a), the approximate first moments (means) computed as

$$\hat{z}_{k|k-1} = E\{\hat{z}_{k|k-1}\} \approx \frac{1}{n_d} \sum_{i=1}^{n_d} z^i_{k|k-1}$$

$$\hat{\boldsymbol{\varepsilon}}_k = E\{\boldsymbol{\varepsilon}_k\} \approx \frac{1}{n_d} \sum_{i=1}^{n_d} \boldsymbol{\varepsilon}^i_k = \hat{z}_{k|k-1} - y_k$$

$$\hat{x}_{k|k-1} = E\{x_{k|k-1}\} \approx \frac{1}{n_d} \sum_{i=1}^{n_d} x^i_{k|k-1}$$

$$\hat{\boldsymbol{\theta}}_{k|k-1} = E\{\boldsymbol{\theta}_{k|k-1}\} \approx \frac{1}{n_d} \sum_{i=1}^{n_d} \boldsymbol{\theta}^i_{k|k-1}$$

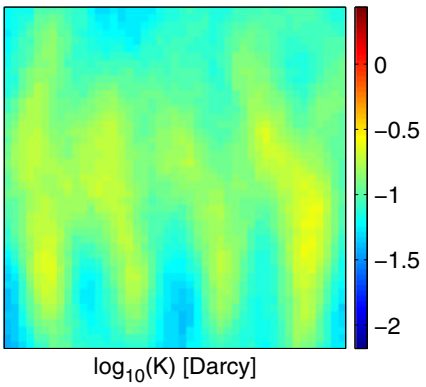

Fig. 4 Permeability mean, $\hat{\boldsymbol{\theta}}_{0|0}$, of the ensemble given in Fig. 3

Table 2 Key indicators for the open-loop optimized cases. Improvements are relative to the nominal case

	NO 10^6 USD	Reactive 10^6 USD, %	Certainty equivalent 10^6 USD, %	RO 10^6 USD, %	RO modified 10^6 USD, %
$E_{\boldsymbol{\theta}}[\psi]$	33.84	56.47, +66.9	42.72, +26.2	44.11, +30.3	58.18, +71.9
Std. dev.	26.35	6.05	18.27	13.19	6.25

and the approximate second moments (covariances) computed by

$$\langle x_{k|k-1}, \boldsymbol{\varepsilon}_k \rangle \approx \frac{1}{n_d - 1} \sum_{i=1}^{n_d} \left(x^i_{k|k-1} - \hat{x}_{k|k-1} \right) \left(\boldsymbol{\varepsilon}^i_k - \hat{\boldsymbol{\varepsilon}}_k \right)'$$

$$\langle \boldsymbol{\theta}_{k|k-1}, \boldsymbol{\varepsilon}_k \rangle \approx \frac{1}{n_d - 1} \sum_{i=1}^{n_d} \left(\boldsymbol{\theta}^i_{k|k-1} - \hat{\boldsymbol{\theta}}_{k|k-1} \right) \left(\boldsymbol{\varepsilon}^i_k - \hat{\boldsymbol{\varepsilon}}_k \right)'$$

$$\langle \boldsymbol{\varepsilon}_k, \boldsymbol{\varepsilon}_k \rangle \approx \frac{1}{n_d - 1} \sum_{i=1}^{n_d} \left(\boldsymbol{\varepsilon}^i_k - \hat{\boldsymbol{\varepsilon}}_k \right) \left(\boldsymbol{\varepsilon}^i_k - \hat{\boldsymbol{\varepsilon}}_k \right)'$$

The result of (23a) in this procedure is an ensemble

$$\left\{ x^i_{k|k}, \boldsymbol{\theta}^i_{k|k} \right\}_{i=1}^{n_d} \quad k = 1, 2, \ldots \tag{28}$$

representing the states and parameters at time k given measurements up until time k. Using this ensemble, a robust optimization may be performed or various statistics such as the mean may be computed.

(23a) may result in non-physical updates. Therefore, we modify the EnKF such that the ensemble (28) satisfies physical constraints, e.g. that the permeabilities are in certain ranges. To mitigate such effects, we clip the solution according to the constraints

$$\boldsymbol{\theta}^i_{k|k} := \begin{cases} \boldsymbol{\theta}_{\min} & \boldsymbol{\theta}^i_{k|k} < \boldsymbol{\theta}_{\min} \\ \boldsymbol{\theta}^i_{k|k} & \boldsymbol{\theta}_{\min} \leq \boldsymbol{\theta}^i_{k|k} \leq \boldsymbol{\theta}_{\max} \\ \boldsymbol{\theta}_{\max} & \boldsymbol{\theta}^i_{k|k} > \boldsymbol{\theta}_{\max} \end{cases} \tag{29}$$

and compute the filtered states, $\hat{x}^i_{k|k}$, by solving the dynamic model equations

$$x^i_{j+1|k} = F\left(x^i_{j|k}, u_j, \boldsymbol{\theta}^i_{k|k} \right), \quad x^i_{0|k} = x_0, \quad j = 0, 1, \ldots, k-1 \tag{30}$$

for each ensemble member, $i \in \{1, \ldots, n_d\}$, using the clipped parameter estimates computed by (29). In this way, state updates consistent with the model is guaranteed [35]. In particular, this eliminates the possibility of nonphysical states (nonphysical pressures and saturations). The computational load can potentially be reduced by only doing the initial-value simulation when the estimated saturation and pressure changes passes a certain threshold [39]. The modifications (29) and (30) provides the ensemble (28) that is used for the optimal control computations and for the initiation of the EnKF at the next time step. Finally, the choice of the ensemble size n_d in the EnKF is a topic of research itself [60]. It affects the performance of the filter. In reservoir engineering an ensemble's size of 100 is a common choice based on experience [4], [61]. However, this number is problem dependent and in some cases good results can also be obtained using ensembles with fewer members [61].

4.2 Performance metrics

To measure the convergence of the Kalman filter estimates, we consider the mean standard deviation

$$\sigma_k = \sqrt{\frac{1}{n_p} \left(\frac{1}{n_d - 1} \sum_{i=1}^{n_d} \left\| \boldsymbol{\theta}^i_{k|k} - \hat{\boldsymbol{\theta}}_{k|k} \right\|_2^2 \right)} \tag{31}$$

of the parameters in the parameter vector, $\boldsymbol{\theta}_{k|k}$. σ_k measures the ensemble spread. We also consider the root-mean-square-error of the parameter estimates compared to the true parameters, $\boldsymbol{\theta}^0$:

$$RMSE_k = \frac{\left\| \hat{\boldsymbol{\theta}}_{k|k} - \boldsymbol{\theta}^0 \right\|_2}{\sqrt{n_p}} \tag{32}$$

$\boldsymbol{\theta}_k$ can be computed for real as well as synthetic cases, while $RMSE_k$ can only be computed for synthetic cases in which the true parameters, $\boldsymbol{\theta}^0$, are available.

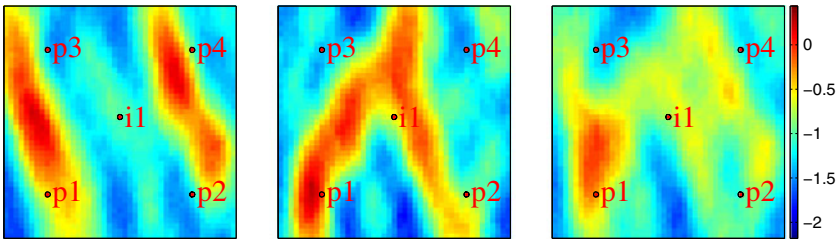

(1) First realization (2) Second realization (3) Ensemble mean

Fig. 5 $\log_{10} K$ [D] of the first two realizations of the ensemble in Fig.3 and their ensemble mean $\hat{\boldsymbol{\theta}}_{0|0}$

In the ideal case, the spread (31) should converge to a number related to the measurement noise and the root-mean-square-error (32) should converge to 0. In practice, (32) will not converge to zero due to e.g. factors like model-plant mismatch. Cases with divergence of the root-mean-square-error may indicate that the ensemble is too small to represent the true uncertainty.

5 Case study

We consider a conventional horizontal oil field that can be modeled as a two phase flow in a porous medium [62–64]. The reservoir size is 450 m × 450 m × 10 m. By spatial discretization this reservoir is divided into 45 × 45 × 1 grid blocks. The permeability field is uncertain. We assume that the ensemble in Fig. 3 represents the range of possible geological uncertainties. The configuration of injection wells and producers is illustrated in Fig. 5(1). As indicated in Fig. 5(1), the four producers are located in the corners of the field, while the single injector is located in the center of the field.

The reservoir's petrophysical parameters are listed in Table 1. The initial reservoir pressure is 300 bar everywhere in the reservoir. The initial water saturation is 0.1 everywhere in the reservoir. This implies that initially, the reservoir has a uniform oil saturation of 0.9. The manipulated variables are the bhp of the five wells (four producers, one injector) over the life of the reservoir. In this study, we consider a zero discount factor d in the cost function (6). This means that we maximize NPV at the final time, without caring about the shorter horizon [11].

The case study is divided into an open-loop optimization part and a closed-loop optimization part. In open-loop optimization, we compute the control strategy without using measurement feedback to update the parameters, i.e. the ensemble in Fig. 3 is fixed in time. In closed-loop optimization, we use production measurements and the EnKF to estimate the permeability field parameters. To simulate the reservoir and create production data, the first realization of the permeability field, $\boldsymbol{\theta}^1_{0|0}$, in Fig. 3 is used. This permeability field represents the true permeability field of the reservoir.

In reality, we never know the true model when performing data assimilation with EnKF. We can only implicitly assume that we can generate a reasonable approximation of the true reservoir. Since we focus on the optimizer formulation and separate the effects of the quality in data assimilation from the quality of CE, RO and reactive strategies as much as possible, we assume that the true reservoir is contained in the ensemble of initial guesses.

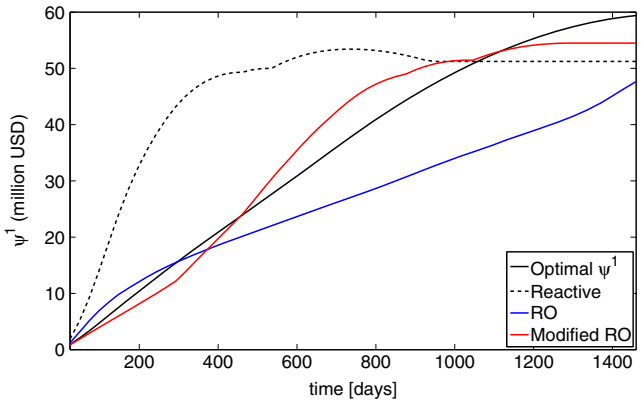

(1) First realization

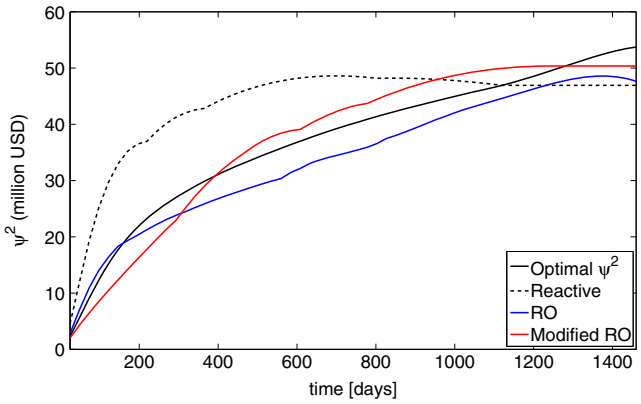

(2) Second realization

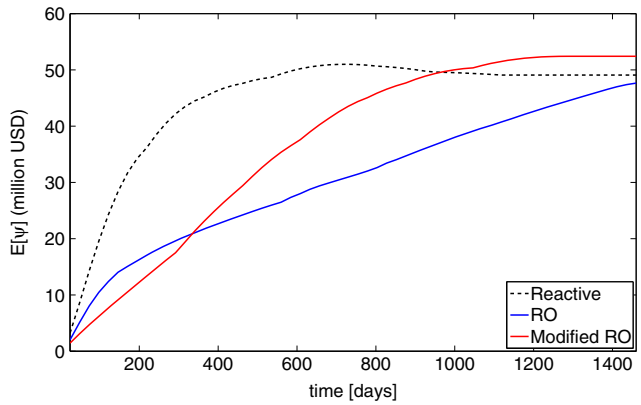

(3) Combined NPV

Fig. 6 Profit evolutions for open-loop optimization of the two ensemble case. The optimal trajectories computed using the true permeability fields give the highest possible profit. The profit of the RO strategy is below the profit of the reactive strategy for the first permeability realization and slightly above the second permeability realization. On average the RO strategy gives less profit than the reactive strategy. The modified RO strategy produces for all cases a higher profit than the reactive strategy

5.1 Open-loop optimization

We consider a prediction horizon of $t_N = 4 \cdot 365 = 1460$ days divided in $N = 60$ control periods (i.e. a control

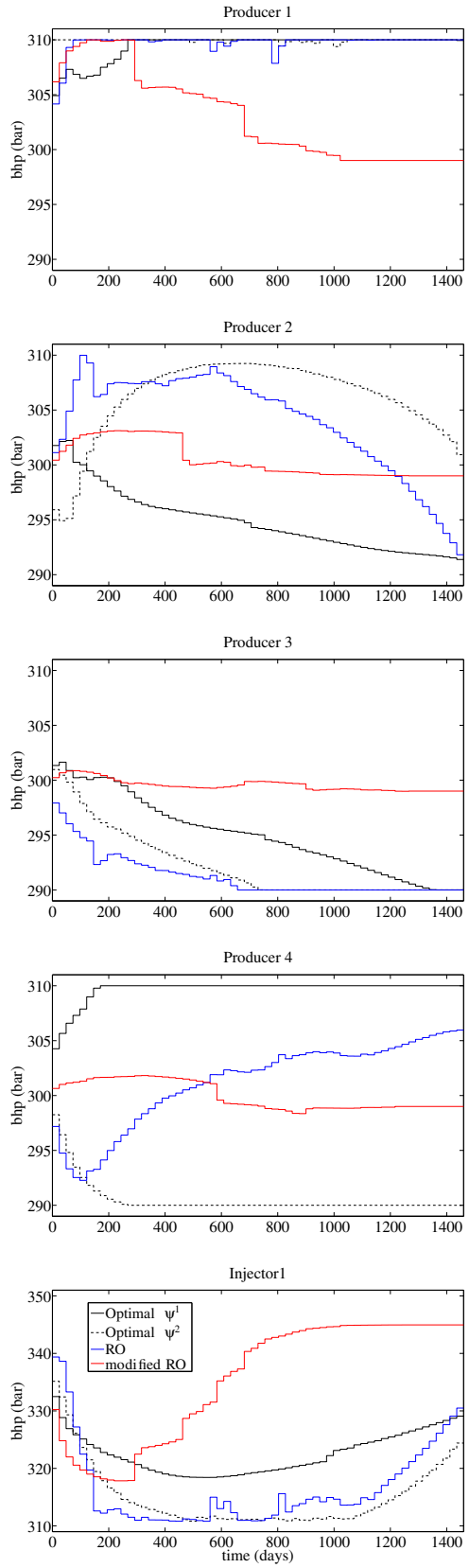

Fig. 7 Control trajectories for open-loop optimization of the two ensemble case. The control trajectories for the considered optimization strategies are very different

period $T_s \approx 24$ days). We control the reservoir using five different strategies that we call: the reactive strategy, the nominal strategy (NO), the certainty equivalent strategy, the robust optimization strategy (RO), and the modified robust optimization strategy (modified RO).

The reactive strategy develops the field at the maximum production rate (setting the producers at the lowest allowed value of 290 bar and the injector at the maximum allowed value of 350 bar) and subsequently shut-in each production well when it is no longer economical. From the values in Table 1, we observe that a producer well becomes uneconomical when the fractional flow f_w is above the value $120/(120 + 20) = 0.857$. The nominal strategy is based on a single realization. For each realization in the ensemble we compute the optimal control trajectory. Then we apply each of these 100 optimal control trajectories to each of the ensemble members obtaining 100 NPV values for each control trajectory. The certainty equivalent strategy is based on solving problem (5a) using the certainty equivalent cost function $\boldsymbol{\psi}_{CE}$ (10). It uses the mean of the ensemble as its permeability field. Figure 4 illustrates the mean of the permeability field ensemble given in Fig. 3. The RO strategy is based on solving problem (5a) using the robust cost function $\boldsymbol{\psi}_{rob}$ (5a) and the robust gradient $\nabla_{u_k}\boldsymbol{\psi}_{rob}$ (15). The modified robust optimization is the RO strategy with an added reactive strategy, i.e. we solve problem (5a) using (14) and (15) but we shut in a producer well when it is non economical. This means that when we solve the flow equations (5c), the number of active producer wells can change. This in turn means that once a well is shut-in, its later contribution to the NPV and its gradient will be zero. We could say that for each realization we manipulate producer wells bhps as long as they are profitable. Further, this strategy stops the production of a reservoir when all wells are non-economical. To our knowledge, there exist no extension of robust optimization that includes reactive control. However, the idea of adding reactive control has been used to improve the NPV of a single reservoir model. In [65] they consider production optimization in the absence of uncertainty by including a watercut constraint on the well completions. This results in increased NPV and a faster convergence of the optimizer.

Simulations reveal that for the present case, the RO strategy yields an higher expected NPV $E_{\boldsymbol{\theta}}[\boldsymbol{\psi}]$ and a lower standard deviation of the NPV (see Table 2) compared to the certainty equivalent strategy. However, both the RO and the certainty equivalent strategies are worse than the reactive strategy because of a much lower expected NPV $E_{\boldsymbol{\theta}}[\boldsymbol{\psi}]$ with a much higher NPV standard deviation. The modified RO strategy has a NPV standard deviation comparable to the reactive strategy, but a higher expected NPV $E_{\boldsymbol{\theta}}[\boldsymbol{\psi}]$. It is important to stress that the results concerning the merits of the different strategies are particular to this case study and

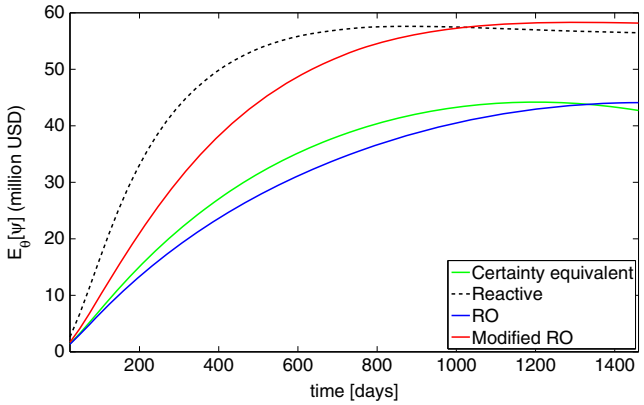

Fig. 8 Profit evolution for open-loop optimization in the hundred ensemble case

not universal. [26] presents a case in which the RO strategy provides higher expected NPV and lower NPV standard deviation than the reactive strategy. In making a comparison with [26], there are a number of things we should stress. First of all, in [26] they are controlling directly the liquid rates of 12 wells with no direct control on the bhp values. In our test case, we control the bhp values of only 5 wells with no direct control on the liquid rates. In [26], all the realizations are giving positive NPV for all the control strategies. Further, they find that the reactive strategy is the worst to use. In our test case, the NO strategy is the worst to use, and it gives a substantial negative NPV contribution. Hence, it seems like the test case in [26] facilitates optimal control strategies. In our case, however, the heterogeneities in the ensemble realizations make it hard for optimal control strategies to improve on a reactive strategy. To summarize, the problems treated in [26] and in this paper have quite different characteristics. Hence, different preferences with respect to open-loop strategies is not necessarily surprising.

The results in our paper indicates the value of feedback. The reactive strategy as well as the modified robust strategy both use a simple form of feedback. The nominal strategy, the certainty equivalent strategy, and the robust optimization strategy are pure open-loop strategies that do not use feedback.

To illustrate the results in a tutorial way, we split the discussion of the open-loop optimization into a two ensemble case and a hundred ensemble case. In the two ensemble case, we present the results of open-loop optimization using an ensemble of two realizations. Figure 5 illustrates the two realizations of the uncertain permeability field for this case. In the case with hundred ensemble members, we use the entire ensemble in Fig. 3 to represent the uncertain permeability field.

5.1.1 Case - ensemble with two members

In this subsection, we describe the performance of the RO strategy for the case with an ensemble consisting of the two permeability field realizations illustrated in Fig. 5. We compare the results of the RO control strategy with the results of the reactive, the modified RO and the optimal control strategies. By the optimal control strategies for the two realizations in Fig. 5, we mean the optimal control strategies, $\{u_k\}_{k=0}^{N-1}$, that are computed by solving the optimization problem (8) using the true permeability fields. These are

$$\boldsymbol{\psi} = \boldsymbol{\psi}\left(\{u_k\}_{k=0}^{N-1}; \bar{x}_0, \boldsymbol{\theta}^1\right) = \boldsymbol{\psi}^1$$
$$\boldsymbol{\psi} = \boldsymbol{\psi}\left(\{u_k\}_{k=0}^{N-1}; \bar{x}_0, \boldsymbol{\theta}^2\right) = \boldsymbol{\psi}^2$$

The NPVs computed using these optimal control strategies act as an upper bound for the NPVs computed using the other control strategies. To choose the two realizations to use, we first compute optimal control trajectories for the realizations in the ensemble of Fig. 3. Then we choose two

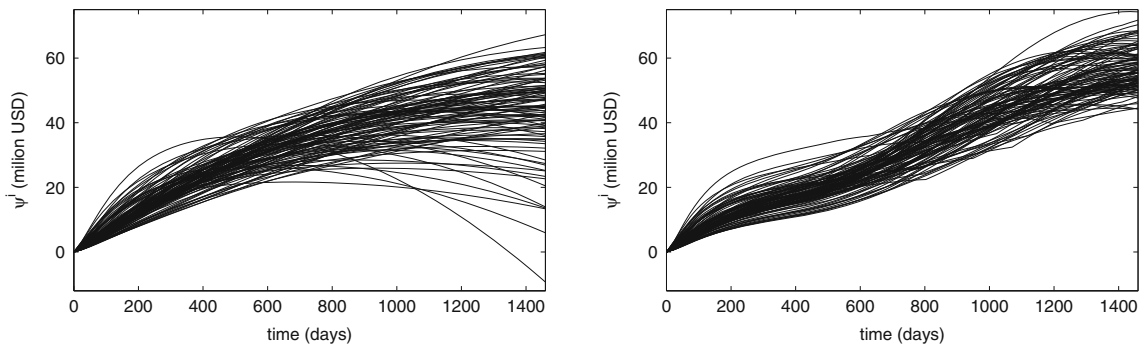

(1) RO strategy (2) Modified RO strategy

Fig. 9 Profit evolution of the open-loop RO strategy and the open-loop modified RO-strategy for each realization of the permeability field. Some scenarios in the RO strategy gives negative profits while the modified RO strategy avoids that by shutting in uneconomical producer wells

realizations with large differences in the optimal production strategies.

Figures 6(1), 6(2) and 6(3) show the terms ψ^1, ψ^2 and $E_\theta[\psi]$ (13) for the reactive strategy, the RO strategy, and the modified RO strategy, respectively. As expected, the NPVs computed using the optimal control strategies give the highest values for ψ^1 and ψ^2. Compared to the reactive strategy, the RO strategy gives a lower NPV, ψ^1, for realization 1, and a higher NPV, ψ^2, for realization 2. As illustrated in Fig. 6(3), this results in a lower NPV mean, $E_\theta[\psi]$, for the RO strategy compared to the reactive strategy. The modified RO control strategy gives the highest NPVs for all the realizations.

Furthermore, it is interesting to observe the difference in production times for the different strategies. For the RO strategy, the production continue for the entire time horizon (1460 days) considered. In the reactive strategy, the production lasts 949 days in the first realization (ψ^2) and 1119 days in the second realization (ψ^2). So there is an important difference in the field developing time of the two realizations. In the modified RO strategy, the production lasts 1289 days in the first realization and 1240 days in the second

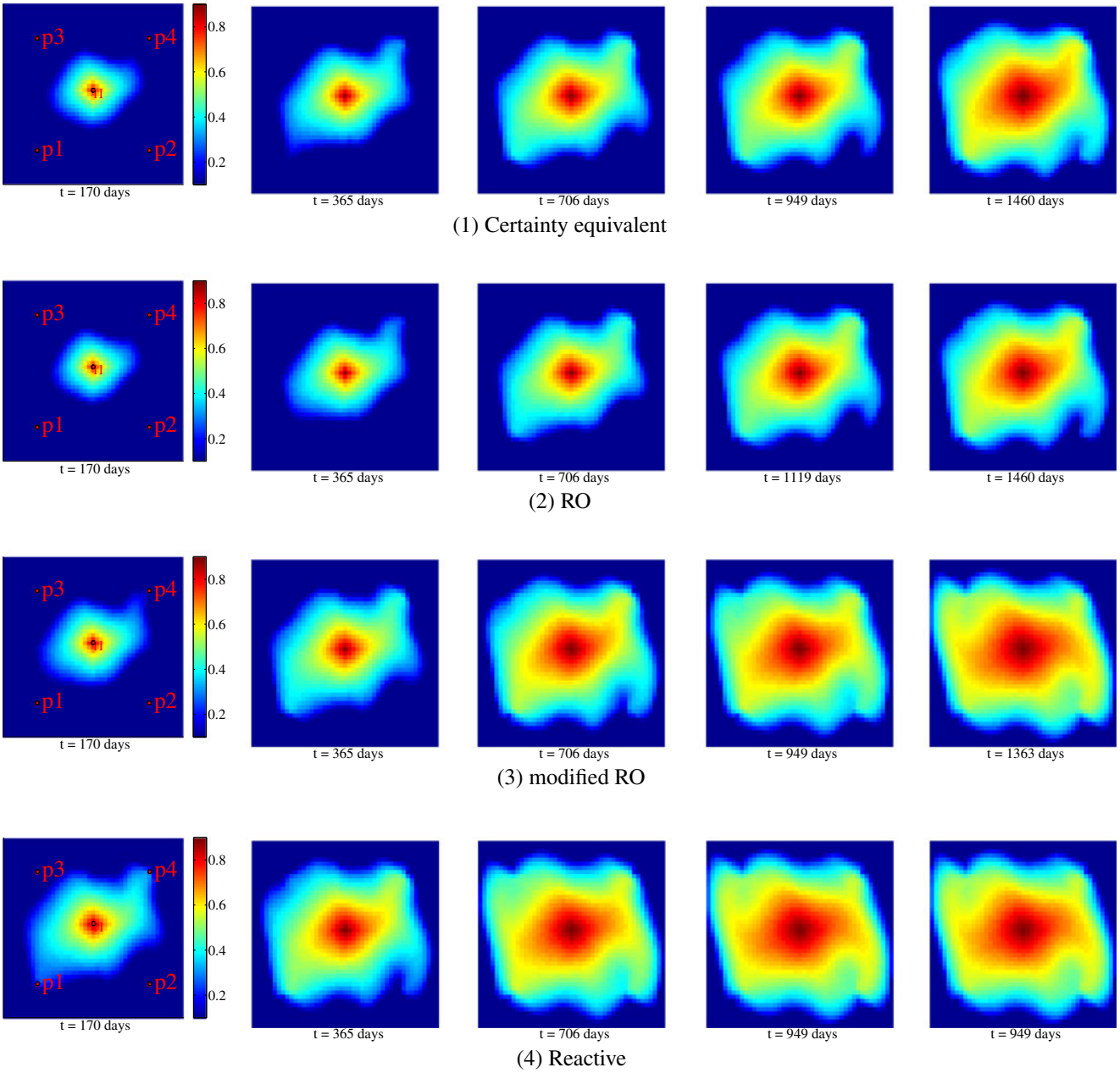

Fig. 10 Saturation profiles of the first realization for the open-loop optimization strategies in the hundred ensemble case

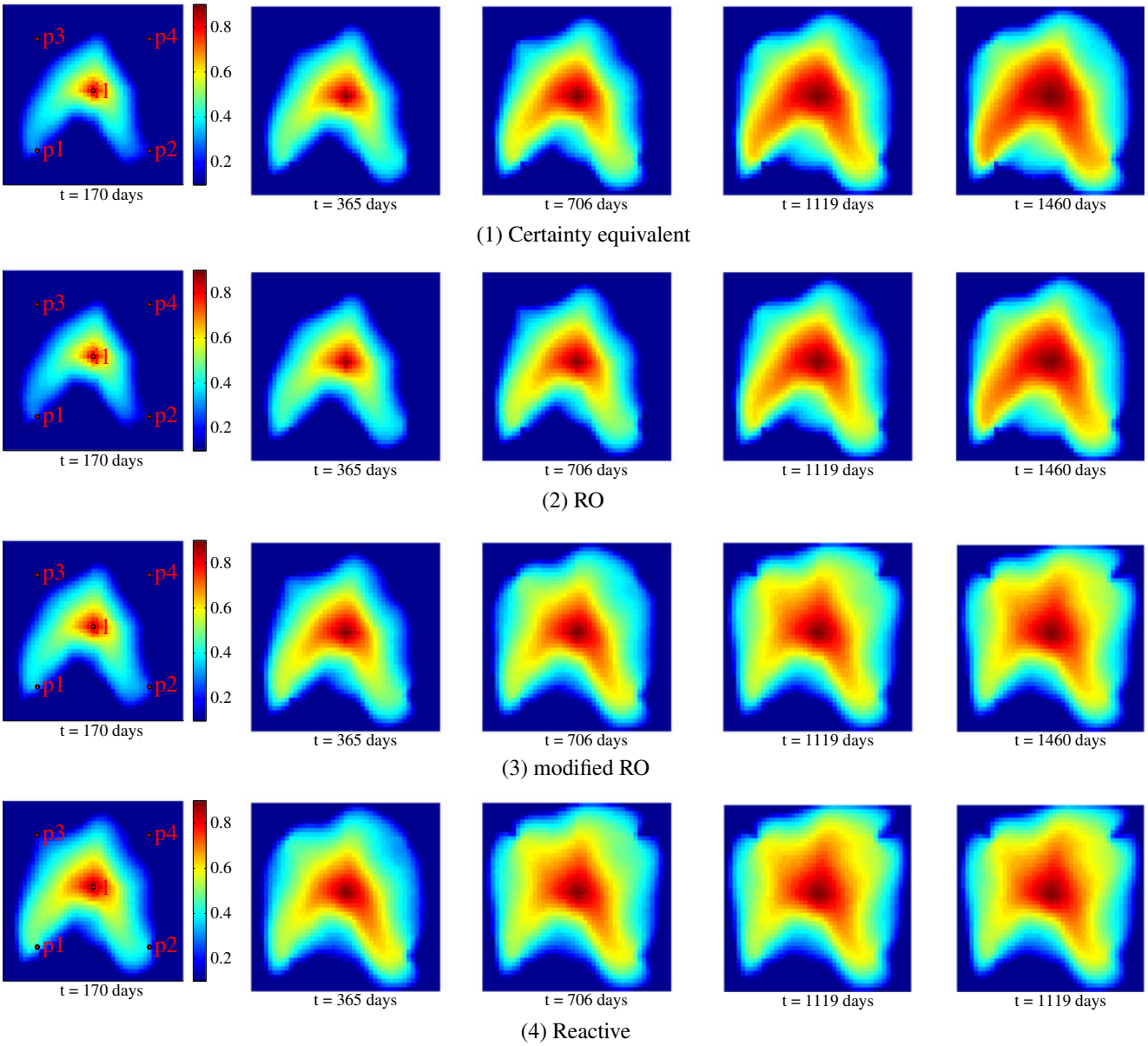

Fig. 11 Saturation profiles of the second realization for the open-loop optimization strategies in the hundred ensemble case

realization. We note that with the modified RO strategy, the production time is longer than the production time of the reactive strategy.

Figure 7 shows the control trajectories of the RO, the modified RO and the optimal strategies. We note that because of the heterogeneity between the realizations, the resulting optimal control trajectory of one realization can be very different and conflicting with the optimal control trajectory for the other realization. To find a common optimal control that takes all these differences into account can be difficult if not impossible. Especially if we don't allow for changes in the configuration of active wells, e.g. producer number 4 is producing at its minimum (310 bar) in the solution for ensemble 1 and at its maximum (290 bar) in the solution for ensemble 2. The RO and modified RO solutions for the producer number 4 stay in between the two optimal trajectories.

In conclusion, the two-ensemble case demonstrates that the optimizer produces the maximal profit for the optimal cases. Therefore, the optimizer works well and the lower profit of the RO strategy is not the result of lack of convergence in the optimizer, but rather the result of heterogeneous permeability fields giving conflicting control trajectories.

5.1.2 Case - ensemble with hundred members

In this subsection, we describe the results for the case in which we do open-loop optimization using the entire

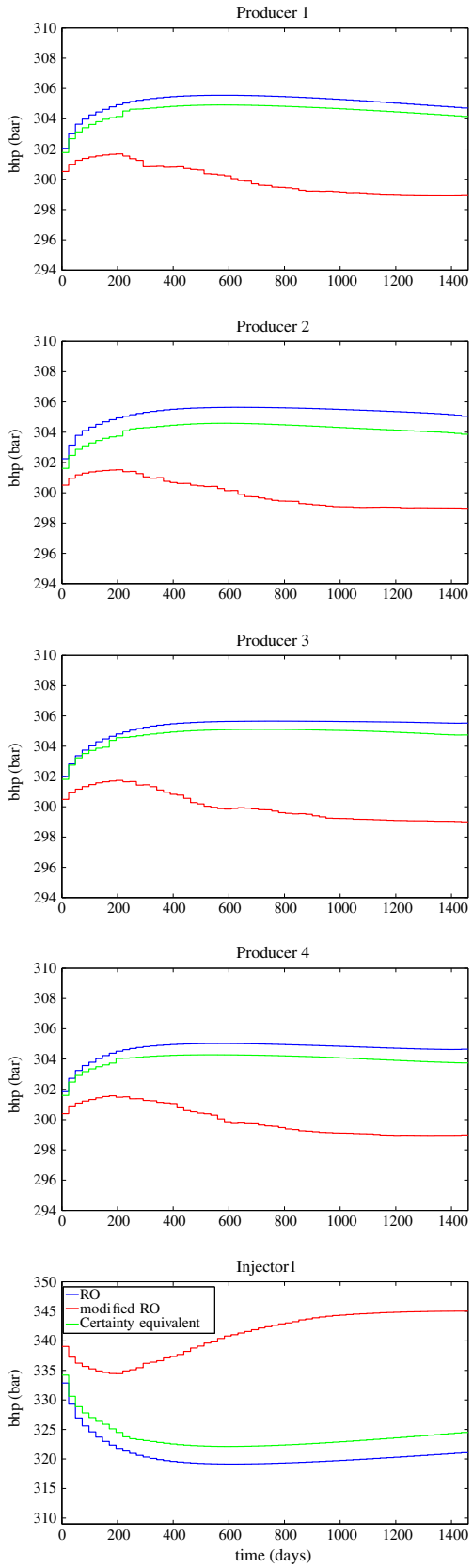

Fig. 12 Control trajectories for open-loop optimization in the hundred ensemble case

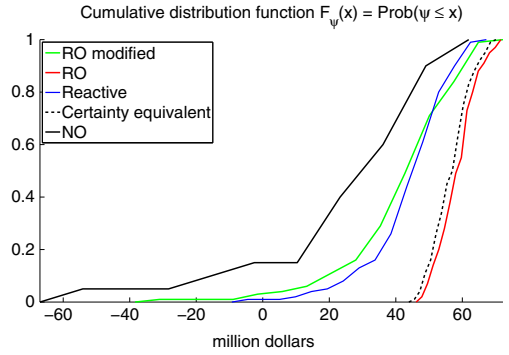

Fig. 13 Cumulative distribution function for the open-loop optimization strategies. The cumulative distribution functions are for the ensemble with hundred members

ensemble of 100 realizations in Fig. 3. Figure 4 illustrates the mean permeability field for the ensemble of permeability fields in Fig. 3. Figure 8 shows the profit evolution in the case of an ensemble consisting of 100 permeability fields for the certainty equivalent strategy, the reactive strategy, the RO strategy, and the the modified RO strategy.

Table 2 reports the corresponding key performance indicators (expected NPV $E_{\theta}[\psi]$ and standard deviation of the NPV). As in the two ensemble case, the reactive strategy yields both a larger expected NPV and a smaller standard deviation for the NPV compared to the certainty equivalent and the the RO strategies. The reasons for the inferior performance of the RO strategy should be searched in the conflicting controls required for the different realizations. Figure 9(1) shows that the RO strategy cannot avoid that some ψ^i gives a negative contribution to the expected NPV

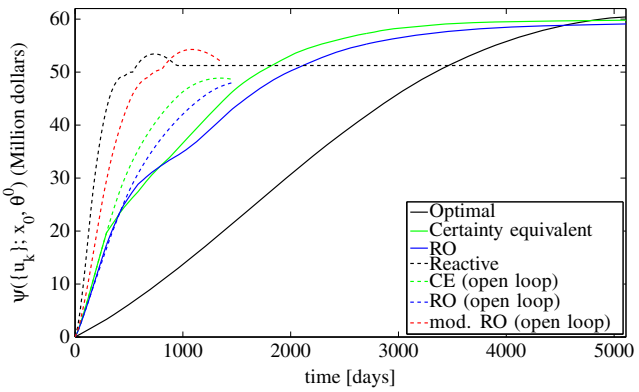

Fig. 14 Profit evolution for the closed-loop optimization strategies. The profit evolution of the true model controlled by different strategies based on the ensemble in Fig. 3. Both the RO and the certainty equivalent strategies give a higher NPV than the the reactive strategy. The optimal control strategy represents the best possible solution. By using the RO strategy and the certainty equivalent strategy we get profits close to the maximum possible profit

Table 3 Key indicators for the closed-loop optimized cases. Improvements are relative to the reactive case

Meas. noise	Reactive	Certainty equivalent		RO		Optimal	
	10^6 USD	10^6 USD, %		10^6 USD, %		10^6 USD, %	
$5 \cdot R$	51.24	59.13,	+15.4	58.34,	+13.9	60.41,	+17.3
R	51.24	59.79,	+16.7	59.09,	+15.3	60.41,	+17.3
$5^{-1} \cdot R$	51.24	59.84,	+16.8	59.52,	+16.2	60.41,	+17.3
$5^{-2} \cdot R$	51.24	59.95,	+17.0	59.56,	+16.2	60.41,	+17.3

$E_{\boldsymbol{\theta}}[\boldsymbol{\psi}]$. In contrast, as illustrated in Fig. 9(2), the modified RO strategy does not produce realizations with negative profit. Furthermore, each realization of the modified RO strategy seems to increase the profit compared to the RO strategy. The reactive strategy performs better than both the RO and ceratinty equivalent strategies because it can shut in a well when it is no longer profitable to operate the well. The modified RO strategy inherits the ability of the reactive strategy to shut in unprofitable wells. This is in essence a simple feedback mechanism. Figures 10 and 11 show the saturation profiles of the first two realizations for the open-loop strategies. We note that the reactive strategy and the modified strategy inject a higher water quantity and displace the oil more uniformly compared to the RO and the certainty equivalent strategies.

Figures 12 shows the control trajectories of the RO, the modified RO and the certainty equivalent strategies. Compared to the the trajectories in Fig. 7, for the two ensemble case, it seems that the RO and certainty equivalent strategies include some averaging (smoothing) in the resulting control trajectories that limits their effectiveness. The result is a control trajectory that produces less oil than the modified RO strategy that can shut in uneconomical producer wells.

As indicated by Fig. 7, the RO control trajectories may be the average of conflicting control trajectories and therefore inefficient for the uncertain system.

Figure 13 shows the cumulative distribution function for the different control strategies, i.e. the probability to get a NPV $\leqslant x$. These curves are similar to the ones reported in [26] with the difference that the NO and the certainty equivalent strategies have a positive probability of giving negative NPVs. Figure 13 confirms that the modified RO strategy is superior to the other open-loop strategies.

5.2 Closed-loop optimization

The closed-loop optimization strategies are implemented using the moving horizon principle. In this method, each time new measurements from the real or simulated reservoir are available, the EnKF uses these measurements to update the estimates of the permeability field, and an open-loop optimization problem is solved using the updated permeability field. Only the first part of the resulting optimal control trajectory is implemented. As new measurements becomes available, the procedure is repeated. The sampling time for the system is $T_s = 146$ days, i.e. the data assimilation and optimization is performed every 146 days. The open-loop optimization uses a prediction and control horizon of $4 \cdot 365 = 1460$ days that is divided into $N = 60$ periods (the same as for the open-loop optimization strategies). With this parametrization, the control steps for the first six periods are implemented to the system, and then

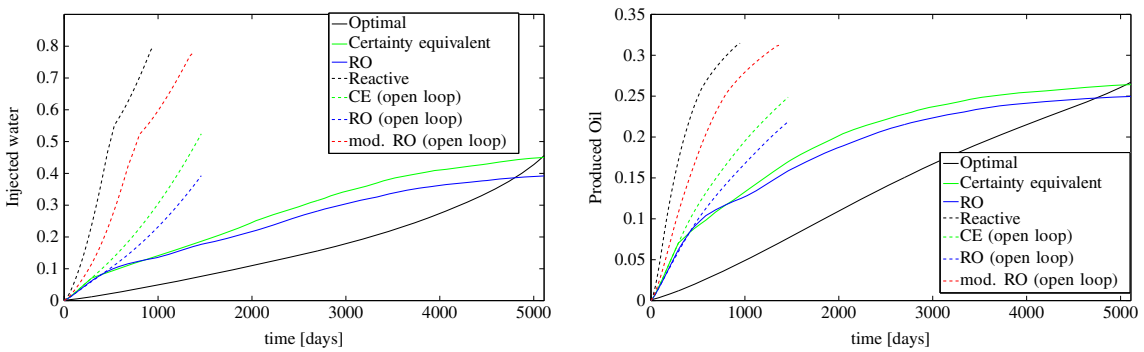

(1) Cumulative water injection (2) Cumulative oil production

Fig. 15 Closed-loop. Water injected and produced oil trajectories for different optimization strategies. The values are normalized with respect to the pore volume

we receive new measurements to do new data assimilation and optimization computations for a shifted time window. In this paper, we consider 35 of these steps such that the total production horizon is $146 \cdot 35 = 5110$ days.

We compare three closed-loop optimization strategies: A reactive strategy, a certainty equivalent strategy, and a RO strategy. We did not implement a modified RO strategy because that would be complicated by the need to manage

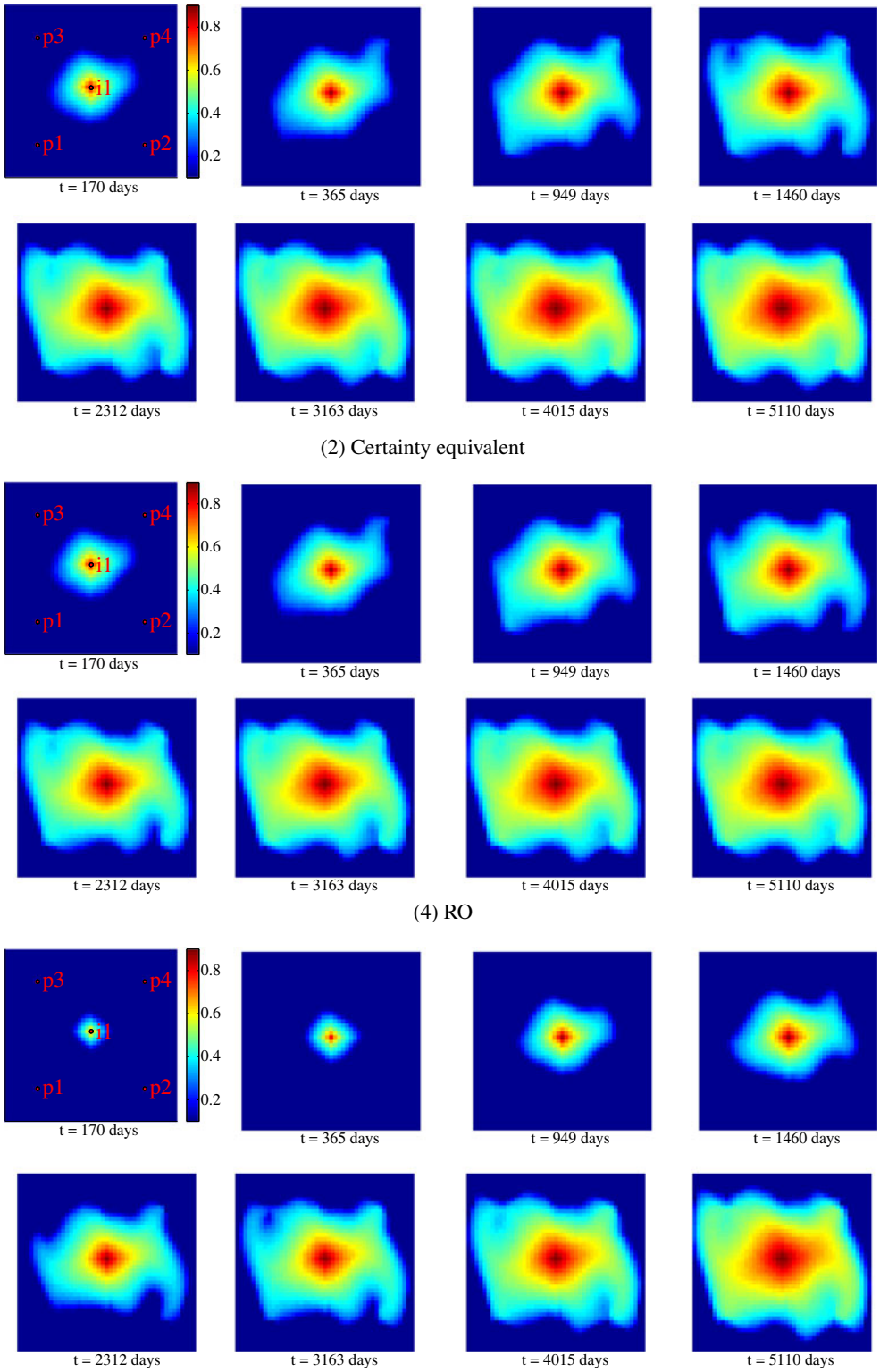

Fig. 16 Saturation profiles of the true field for the closed-loop optimization strategies

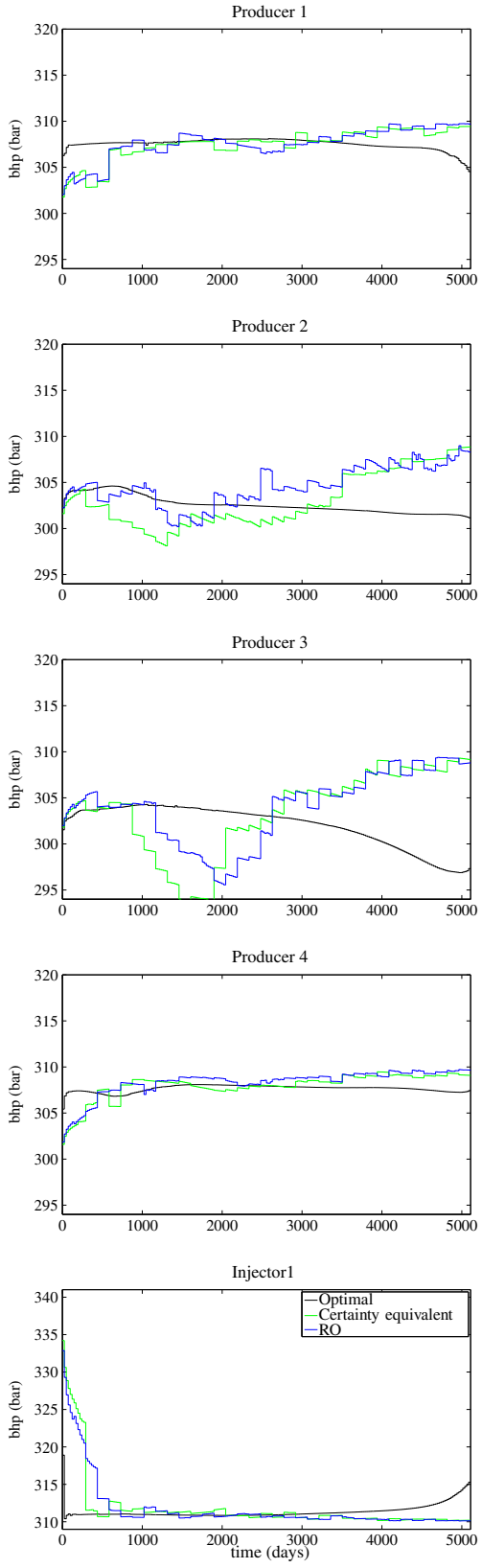

Fig. 17 Control trajectories for the closed-loop optimization strategies

situations with a variable number of active wells and measurements for different ensemble realizations. Further, it would require a strategy to replace ensemble realizations when all the producing wells are shut-in.

Figure 14 shows the NPV $\boldsymbol{\psi}\left(\{u_k\}_{k=0}^{N-1}; x_0, \boldsymbol{\theta}_{0|0}^1\right)$ for the reactive strategy, the closed-loop RO strategy, the closed-loop certainty equivalent strategy, the optimal control strategy, and the open-loop strategies introduced in the previous section. The optimal control strategy is obtained solving the optimization problem (7) using the true permeability field (the first realization of the permeability field in Fig. 3). The NPV computed by the optimal control strategy represents the best possible operation of the reservoir. Table 3 reports key indicators (expected NPV and improvements compared to the reactive strategy) for the closed-loop strategies at different levels of measurement noise. Figure 14 and Table 3 shows that for all investigated cases, both the closed-loop certainty equivalent strategy and the closed-loop RO strategy yields significantly higher NPV than the reactive strategy. As is also evident from Fig. 14 and Table 3, the closed-loop certainty equivalent strategy

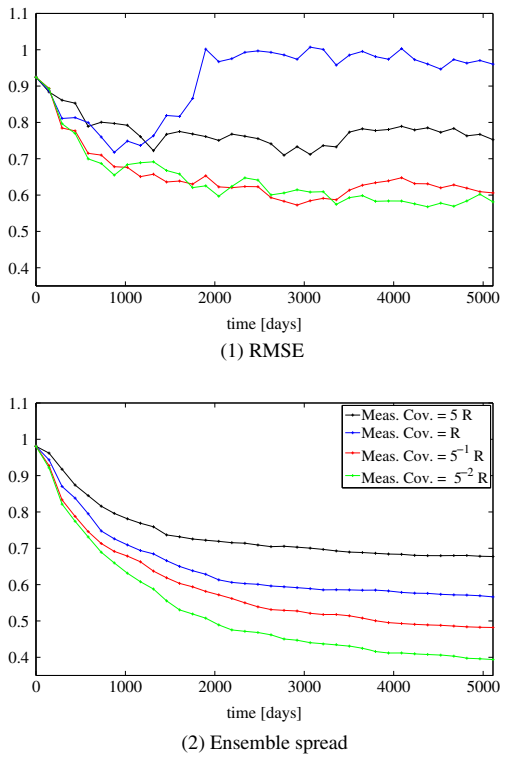

Fig. 18 Convergence measures for the EnKF with various levels of measurement noise for the closed-loop certainty equivalent strategy. (1) shows that the EnKF does not converge to the true parameters. However, the estimate captures enough features to be useful. (2) illustrates that the parameter uncertainty decreases as more production data is assimilated in the estimates

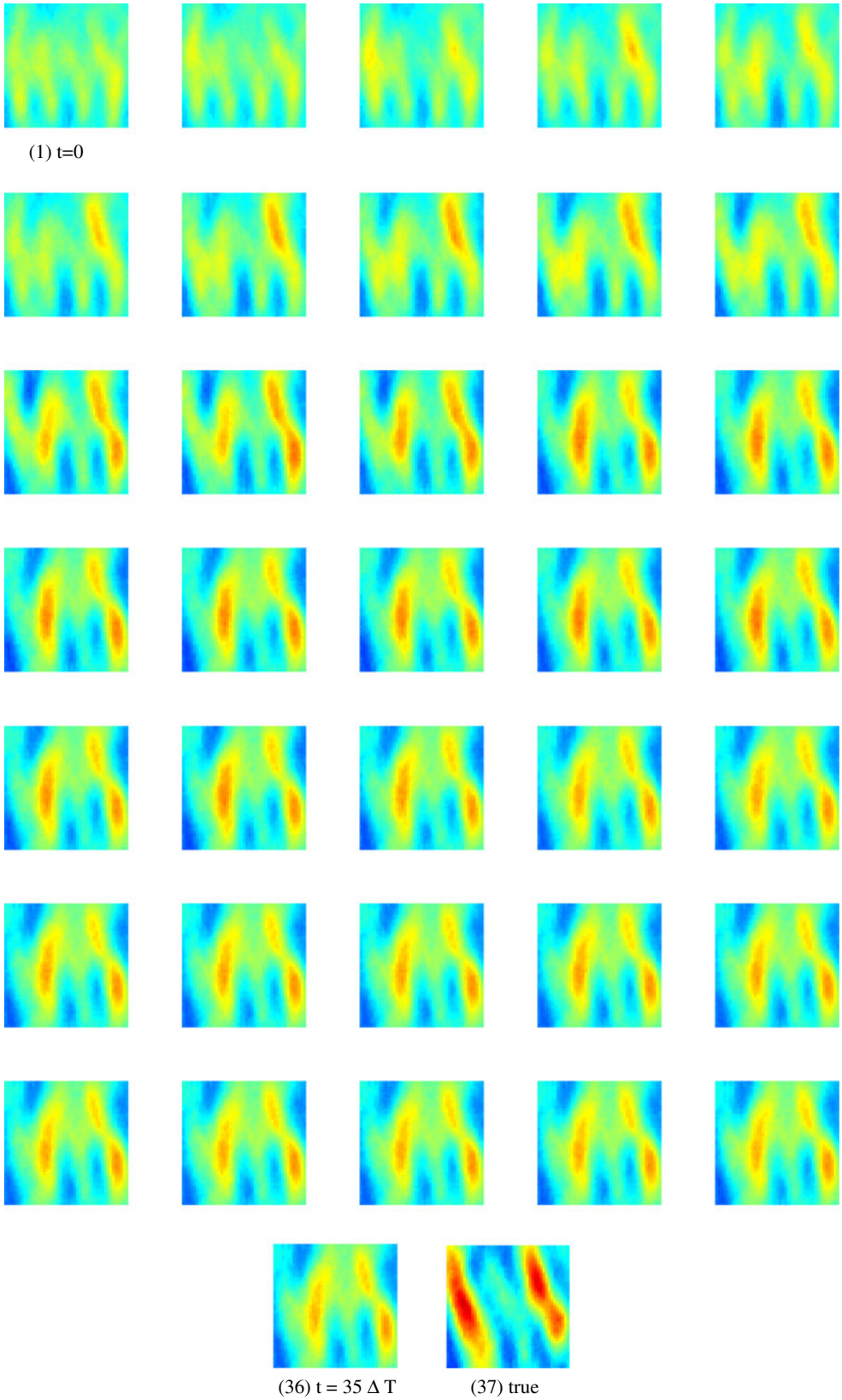

Fig. 19 Estimates of the mean permeability field as function of time for the closed-loop certainty equivalent strategy. The initial estimate is a four channel structure. The estimates, $\hat{\boldsymbol{\theta}}_{k|k-1}$, converge towards the true two-channel structure as more measurements are assimilated

yields higher NPV than the closed-loop RO strategy. Furthermore, the NPV of the closed-loop certainty equivalent strategy is very close to the NPV of the optimal strategy. Consequently, the closed-loop certainty equivalent strategy is preferable over the closed-loop RO strategy as it yields higher NPV and requires significantly less computational effort. This observation is also confirmed when using the second realization in Fig. 3 as the permeability field.

From Fig. 14 we note also that the modified RO is the best open-loop strategy and that the closed-loop strategies CE and RO provide better results compared to the modified RO starting from the assimilation steps 13 ($t \approx 1898$ days) and 16 ($t \approx 2336$ days), respectively. Figure 15 shows the cumulative water injection and the cumulative oil production for different strategies. The slope of the curves is the reservoir injection/production rate. In general, we note that the closed-loop strategies are injecting at a lower rate compared to the open-loop strategies. This happens since we use a zero discount factor, i.e. we focus on long term behaviour. Moreover, there are no direct bounds on the liquid rates. We note that the open-loop strategies, so as the optimal strategy, have an upward concavity. This means that the water injection rate is increasing with time: these strategies increase the injection at the final time to exploit the high oil-to-water price ratio. The closed-loop strategies, instead, have a downward concavity. At the beginning (first 300 days) the closed-loop strategies are injecting at a similar pace as their open-loop counterparts (same slope in the initial part of the curves). However, as the data assimilation proceed, and a better estimate of the true field is given, the closed-loop strategies try to inject/produce as much as the optimal strategy (black curves in figure). This explains the change in concavity of the closed-loop strategies i.e. why the closed-loop strategies reduce the water injection rate with time. Figure 16 illustrates the saturation profiles of the true field for the closed-loop strategies. We note that they have similar field sweep at the final time. Figure 17 shows the corresponding control trajectories of the different closed-loop control strategies. It is evident that the control trajectories of the optimal control strategy are very different from the control trajectories for the closed-loop certainty equivalent and the closed-loop RO strategies.

Figure 18 illustrates the RMSE (32) and the ensemble spread (31) of the EnKF when applied together with the certainty equivalent strategy. The RMSE indicates whether the permeability parameter estimate of the EnKF converges toward the true permeability parameters. The ensemble spread indicates the uncertainty in the estimated permeability parameters. The RMSE and the ensemble spread sequences are computed for different levels of measurement noise, i.e. different values of R in (16b). Figure 18(2) indicates that decreasing levels of measurements noise, R, decrease the ensemble spread (31). This decrease does not always results in a lower RMSE (32) value. However, as is evident from Fig. 18(2), in most of the cases, lower measurement noise levels reduce the RMSE. In this case study there is no ensemble collapse. In fact, Fig. 20 shows that the ensemble realizations have different distances at the last assimilation time, this is an index of the variability in the ensemble of realizations.

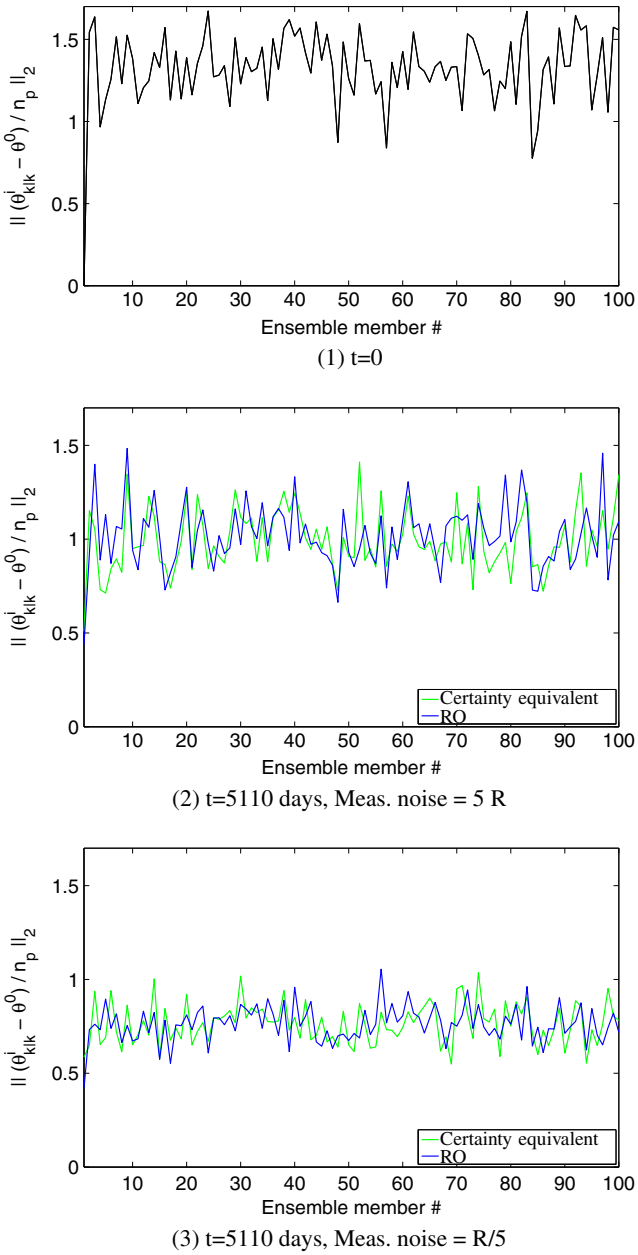

(1) t=0

(2) t=5110 days, Meas. noise = 5 R

(3) t=5110 days, Meas. noise = R/5

Fig. 20 Closed-loop. Distance of the ensemble realizations of the permeability field respect to the true permeability field for (1) the initial ensemble, (2) the final ensemble with a measurement noise of 5 R and (3) the final ensemble with a measurement noise of R/5. We note that also in the case with the lowest measurement noise, the ensemble is not collapsing

In the EnKF, at each data assimilation step, we update the estimated permeability field for each ensemble member. Figure 19 illustrates the time evolution of the mean, $\hat{\boldsymbol{\theta}}_{k|k-1}$, of these estimated permeability field ensembles for the closed-loop certainty equivalent optimization strategy. Figure 19 indicates that the estimated mean permeability field captures the main features of the true permeability field. We start out with a mean permeability field having four channel structures and converge towards the correct two channel structure. Figure 20 illustrates the associated uncertainty with this permeability estimate.

6 Conclusions

In this paper, we demonstrate the open-loop and the closed-loop performance of the certainty equivalent strategy and the RO strategy. For the open-loop case we present a modified RO strategy that performs significantly better than the other open-loop strategies. In the closed-loop situation for the case studied, we arrive at the surprising conclusion that the certainty equivalent strategy is slightly better than the RO strategy.

For the case presented, the open-loop RO strategy yields 3 % higher expected NPV and 28 % lower NPV standard deviation than the open-loop certainty equivalent strategy. Yet, the reactive strategy performed even better than the open-loop RO strategy. Simulations indicate that the inferior performance of the open-loop RO strategy compared to the reactive strategy is due to the inability of the RO strategy to efficiently encompass ensembles with very different and conflicting optimal control trajectories. We propose a modified RO strategy that allow shut in of uneconomical wells. The modified RO strategy performs significantly better than the other open-loop strategies and the reactive strategy. The modified RO optimization strategy yields an expected NPV that is 36 % higher than the expected NPV of the open-loop certainty equivalent strategy and 3 % higher than the expected NPV for the reactive strategy. The NPV standard deviation of the modified RO strategy is similar to the NPV standard deviation of the reactive strategy. These observations are non-trivial, as previous literature suggests that the open-loop RO strategy performs better than the reactive strategy [26]. The improved economic performance of the open-loop modified RO strategy justifies the computational effort used in determining the trajectories for this strategy.

The simulations for the closed-loop strategies, reveal that the RO strategy and the certainty equivalent strategy yields significantly higher NPV than the reactive strategy. Surprisingly, the closed-loop certainty equivalent strategy yields a higher NPV than the closed-loop RO strategy for the case studied. The uncertainty reduction of the permeability field estimate due to data assimilation explains the good performance of the closed-loop certainty equivalent optimization strategy. Consequently, in closed-loop, the increased computational effort of the RO strategy compared to the certainty equivalent strategy is not justified for the particular case studied in this paper.

Future work will include a test of the strategies discussed in this paper on a more complex scenario (many wells, 3D grid, state/output constraints, spurious correlations), and we plan to work on the "Brugge field" [28]. In open-loop simulations, we expect that the modified RO strategy will improve the RO strategy as seen here. This result is in some way anticipated in [65], where, despite they do not consider uncertainty in the reservoir parameters, they get an increased NPV for the "Brugge field" by adding a reactive control to an optimal control strategy. In closed-loop simulations, we expect to obtain similar results for the RO and the CE strategies provided the data assimilation converges properly, as in the case showed in this paper. Finally, the optimization strategies presented in this paper and to our knowledge all literature on closed-loop reservoir management deals with optimization of the expected NPV. The approaches only implicitly considers risk and variance of the NPV. Future approaches should more directly include risk and variance of the NPV in the optimization.

Acknowledgments This research project is financially supported by the Danish Research Council for Technology and Production Sciences. FTP Grant no. 274-06-0284 and the Center for Integrated Operations in the Petroleum Industry at NTNU.

References

1. Brouwer, D., Nævdal, G., Jansen, J.: Improved reservoir management through optimal control and continuous model updating. In: SPE Annual Technical Conference and Exhibition, Houston (2004)
2. Brouwer, D.R., Jansen, J.D.: Dynamic optimization of waterflooding with smart wells using optimal control theory. SPE J. **9**, 391–402 (2004)
3. Sarma, P., Durlofsky, L., Aziz, K.: Efficient closed-loop production optimization under uncertainty. In: SPE Europec/EAGE Annual Conference, Madrid (2005)
4. Nævdal, G., Brouwer, D.R., Jansen, J.-D.: Waterflooding using closed-loop control. Comput. Geosci. **10**, 37–60 (2006)
5. Jansen, J.-D., Bosgra, O.H., Van den Hof, P.M.J.: Model-based control of multiphase flow in subsurface oil reservoirs. J. Process Control **18**, 846–855 (2008)
6. Jansen, J.D., et al.: Closed-loop reservoir management. In: 2009 SPE Reservoir Simulation Symposium, SPE 119098 The Woodlands, Texas (2009)
7. Lorentzen, R.J., Shafieirad, A., Nævdal, G.: Closed loop reservoir management using the ensemble Kalman filter and sequential quadratic programming. In: 2009 SPE Reservoir Simulation Symposium, SPE 119101. The Woodlands, Texas (2009)
8. Foss, B., Jensen, J.P.: Performance analysis for closed-loop reservoir management. SPE J. **16**, 183–190 (2011)
9. Capolei, A., Stenby, E.H., Jørgensen, J.B.: High order adjoint derivatives using esdirk methods for oil reservoir production

optimization. In: ECMOR XIII 13th European Conference on the Mathematics of Oil Recovery (2012)
10. Van den Hof, P.M.J., Jansen, J.D., Heemink, A.: Recent developments in model-based optimization and control of subsurface flow in oil reservoirs. In: Proceedings of the 2012 IFAC Workshop on Automatic Control in Offshore Oil and Gas Production, pp. 189–200, Trondheim (2012)
11. Capolei, A., Völcker, C., Frydendall, J., Jørgensen, J.B.: Oil reservoir production optimization using single shooting and ESDIRK methods. In: Proceedings of the 2012 IFAC Workshop on Automatic Control in Offshore Oil and Gas Production, pp. 286–291, Trondheim (2012)
12. Foss, B.: Process control in conventional oil and gas fields - challenges and opportunities. Control. Eng. Pract. **20**, 1058–1064 (2012)
13. Rawlings, J.B., Mayne, D.Q.: Model predictive control: Theory and design. Nob Hill Publishing, Madison (2009)
14. Grüne, L., Pannek, J.: Nonlinear model predictive control theory and algorithms. Springer, London (2011)
15. Grötschel, M., Krumke, S.O., Rambau, J. (eds.): Online optimization of large scale systems. Springer, Heidelberg (2001)
16. Allgöwer, F., Zheng, A. (eds.): Nonlinear Model Predictive Control, vol. 26 Progress in Systems and Control Theory. Birkhäuser, Basel (2000)
17. Findeisen, R., Allgöwer, F., Biegler, L.T. (eds.): Assessment and future directions of nonlinear model predictive control. Lecture Notes in Control and Information Sciences, vol. 358, Springer, Heidelberg (2007)
18. Magni, L., Raimondo, D.M., Allgöwer, F. (eds.) : Nonlinear model predictive control. Towards New Challenging Applications. Lecture Notes in Control and Information Sciences, vol. 384, Springer, Heidelberg (2009)
19. Lazar, M., Allgöwer, F. (eds.): 4th IFAC Nonlinear Model Predictive Control Conference (NMPC'12). IFAC Noordwijkerhout, NL (2012)
20. Evensen, G.: Data Assimilation: The Ensemble Kalman Filter, 2nd edn. Springer (2009)
21. Biegler, L.T., Ghattas, O., Heinkenschloss, M., van Bloemen Waanders, B. (eds.): Large-Scale PDE-Constrained Optimization. Springer (2003)
22. Biegler, L.T., Ghattas, O., Heinkenschloss, M., Keyes, D., van Bloemen Waanders, B. (eds.): Real-Time PDE-Constrained Optimization SIAM (2007)
23. Markowitz, H.: Portfolio selection. J. Finance **7**, 77–91 (1952)
24. Terwiesch, P., Ravemark, D., Schenker, B., Rippin, D.W.: Semi-batch process optimization under uncertainty: Theory and experiments. Comput. Chem. Eng. **22**, 201–213 (1998)
25. Srinivasana, B., Bonvina, D., Vissera, E., Palankib, S.: Dynamic optimization of batch processes: II role of measurements in handling uncertainty. Comp. Chem. Eng. **27**, 27–44 (2003)
26. Van Essen, G.M., Zandvliet, M.J., Van den Hof, P.M.J., Bosgra, O.H., Jansen, J.D.: Robust waterflooding optimazation of multiple geological scenarios. SPE J. **14**, 202–210 (2009)
27. Chen, C., Wang, Y., Li, G., Reynolds, A.C.: Closed-loop reservoir management on the Brugge test case. Comput. Geosci. **14**, 691–703 (2010)
28. Peters, L., et al.: Results of the Brugge benchmark study for flooding optimization and history matching. SPE Reserv. Eval. Eng. **13**, 391–405 (2010)
29. Evensen, G.: The ensemble Kalman filter: theoretical formulation and practical implementation. Ocean Dyn. **53**, 342–367 (2003)
30. Wen, X.-H., Chen, W.H.: Some practical issues on real-time reservoir model updating using ensemble Kalman filter. SPE J. **12**, 156–166 (2007)
31. Ehrendorfer, M.: A review of issues in ensemble-based Kalman filtering. Meteorol. Z. **16**, 795–818 (2007)
32. Aanonsen, S.I., Nævdal G., Oliver, D.S., Reynolds, A.C., Valls, B.: The ensemble Kalman filter in reservoir engineering-a review. SPE J. **14**, 393–412 (2009)
33. Simon, D.: Optimal State Estimation Kalman, H_∞, and Nonlinear Approaches. Wiley, Hoboken (2006)
34. Rawlings, J.B., Bakshi, B.R.: Particle filtering and moving horizon estimation. Comput. Chem. Eng. **30**, 1529–1541 (2006)
35. Wen, X.-H., Chen, W.H.: Real-time reservoir model updating using ensemble Kalman filter with confirming option. SPE J. **11**, 431–442 (2006)
36. Sarma, P., Chen, W. Preventing ensemble collapse and preserving geostatistical variability across the ensemble with the subspace enkf. In: ECMOR XIII-13th European Conference on the Mathematics of Oil Recovery. Biarritx, France (2012)
37. Sarma, P., Chen, W.H. Robust and efficient handling of model contraints with the kernal-based ensemble Kalman filter. In: Reservoir Simulation Symposium. The Woodlands, Texas (2011)
38. Sarma, P., Chen, W. Generalization of the ensemble Kalman filter using kernels for nongaussian random fields. In: SPE Reservoir Simulation Symposium. The Woodlands, Texas (2009)
39. Chen, Y., Oliver, D.S., Zhang, D.: Efficient ensemble-based closed-loop production optimization. SPE J. **14**, 634–645 (2009)
40. Chen, Y., Oliver, D.S.: Ensemble-based closed-loop optimization applied to Brugge field. SPE Reserv. Eval. Eng. **13**, 56–71 (2010)
41. Lie, K.A., et al.: Open source matlab implementation of consistent discretisations on complex grids. Comput. Geosci. **16**, 297–322 (2012)
42. Peaceman, D.W.: Interpretation of well-block pressures in numerical reservoir simulation with nonsquare grid blocks and anisotropic permeability. SPE J. **23**(3), 531-543 (1983)
43. Suwartadi, E., Krogstad, S., Foss, B.: Nonlinear output constraints handling for production optimization of oil reservoirs. Comput. Geosci. **16**, 499–517 (2012)
44. Schlegel, M., Stockmann, K., Binder, T., Marquardt, W.: Dynamic optimization using adaptive control vector parameterization. Comput. Chem. Eng. **29**, 1731–1751 (2005)
45. Capolei, A., Jørgensen, J.B. Solution of constrained optimal control problems using multiple shooting and esdirk methods. In: American Control Conference (ACC), 295–300 (2012)
46. Bock, H.G., Plitt, K.J. A multiple shooting algorithm for direct solution of optimal control problems. In: Proceedings 9th IFAC World Congress Budapest, pp. 243–247. Pergamon Press (1984)
47. Biegler, L.T.: Solution of dynamic optimization problems by successive quadratic programming and orthogonal collocation. Comput. Chem. Eng. **8**, 243–248 (1984)
48. Jansen, J.: Adjoint-based optimization of multi-phase flow through porous media - A review. Comput. Fluids **46**, 40–51 (2011)
49. Sarma, P., Aziz, K., Durlofsky, L.J. Implementation of adjoint solution for optimal control of smart wells. In: SPE Reservoir Simulation Symposium, 31 January-2 Feburary 2005, The Woodlands, Texas (2005)
50. Jørgensen, J.B. Adjoint sensitivity results for predictive control, state- and parameter-estimation with nonlinear models. In: Proceedings of the European Control Conference 2007, pp. 3649–3656. Kos, Greece (2007)
51. Völcker, C., Jørgensen, J.B., Stenby, E.H. Oil reservoir production optimization using optimal control. In: 50th IEEE Conference on Decision and Control and European Control Conference, 7937–7943 Orlando, Florida (2011)

52. Byrd, R.H., Nocedal, J., Waltz, R.A.: Knitro: An integrated package for nonlinear optimization. In: Large Scale Nonlinear Optimization, pp. 35–59 (2006)
53. MATLAB. version 7.13.0.564 (R2011b) (The MathWorks Inc., Natick, Massachusetts, 2011)
54. Liu, Y.: Using the snesim program for multiple-point statistical simulation. Comput. Geosci. **32**, 1544–1563 (2006)
55. Schölkopf, B., Smola, A., Müller, K.-R.: Nonlinear component analysis as a kernel eigenvalue problem. Neural Comput. **10**, 1299–1319 (1998)
56. Kalman, R.E.: A new approach to linear filtering and predictions problems. J. Basic Eng. **82**, 35–45 (1960)
57. Kailath, T., Sayed, A.H., Hassibi, B.: Linear Estimation. Prentice Hall (2000)
58. Jazwinski, A.H.: Stochastic Processes and Filtering Theory. Academic Press (1970)
59. Burgers, G., van Leeuwen, P.J., Evensen, G.: Analysis scheme in the ensemble Kalman filter. Mon. Weather Rev. **126**, 1719–1724 (1998)
60. Wen, X.H., Chen, W.: Real-time reservoir model updating using ensemble Kalman filter. In: SPE Reservoir Simulation Symposium. The Woodlands, Texas (2005)
61. Gu, Y., Oliver, D.S.: History matching of the punq-s3 reservoir model using the ensemble Kalman filter. SPE J. **10**, 217–224 (2005)
62. Chen, Z. Reservoir Simulation Mathematical Techniques in Oil Recovery. SIAM Philadelphia (2007)
63. Aziz, K., Durlofsky, L., Tchelepi, H.: Notes on petroleum reservoir simulation. Department of Petroleum Engineering School of Earth Sciences, Stanford University (2005)
64. Völcker, C., Jørgensen, J.B., Thomsen, P.G., Stenby, E.H. Simulation of subsurface two-phase flow in an oil reservoir. In: Proceedings of the European Control Conference 2009, pp. 1221–1226. Budapest, Hungary (2009)
65. Dehdari, V., Oliver, D.S.: Sequential quadratic programming for solving constrained production optimization – case study from Brugge field. SPE J. **17**, 874–884 (2012)